

## RESEARCH ARTICLE SUMMARY

## COMMUNITY ECOLOGY

# Diversity begets stability: Sublinear growth and competitive coexistence across ecosystems

Ian A. Hatton<sup>\*†</sup>, Onofrio Mazzarisi<sup>†</sup>, Ada Altieri, Matteo Smerlak

**INTRODUCTION:** The Earth's tropical rainforests and coral reefs are a marvel of biodiversity and stability. For ecologists, however, they present a theoretical puzzle. Early ecologists believed species diversity to be a leading cause of ecological stability, which includes relative constancy in abundance and the ability to recover from disturbance. However, this view runs counter to classic theories and simple ecological models, such as the generalized Lotka-Volterra (GLV) model. The GLV model, along with Robert May's seminal results from random matrix theory, implies that diversity should instead lead to instability. Many studies have since found factors that can extend stability to more diverse competitive communities, but theory has yet to demonstrate how diversity may be the cause of stability, producing a positive diversity-stability relationship. This disconnect between theory and observation, framed as the "diversity-stability debate," casts doubt on ecological model predictions at a time when they are most critically needed.

**RATIONALE:** Although much theory has focused on the varied ways in which species interact with each other, we focus on the nature of population growth and the way in which a species interacts with itself. Many models, including GLV, assume that populations grow exponentially at low densities and saturate at high densities, following the logistic function. However, there is evidence from time-series analysis that many populations of mammals, birds, fish, and insects tend to follow a different trajectory, one in which the growth of populations increases with density raised to a power less than one. This "sublinear" dynamic is thus similar to the widely used Bertalanffy model of individual growth through ontogeny. Here, we contrast the competitive dynamics that result under both the logistic and sublinear growth models. We then confront sublinear model predictions with several macroecological patterns, as well as observations of community recovery from disturbance.



**From tropical rainforests to coral reefs, some of Earth's most diverse ecosystems are also the most stable.** This staggering diversity stands in opposition to ecological theory, which for decades has predicted that diversity begets instability. We show that a small difference in how population growth is formulated can reverse these classic predictions and match theory with observation. [Photos: Rhett Butler and MPI MiS]

**RESULTS:** Although logistic and sublinear growth share similar features at the population level, they lead to opposing predictions at the community level. Whereas logistic growth of populations implies that diversity begets instability, we find that sublinear growth allows the emergence of a form of collective regulation of populations, leading to community coexistence. Furthermore, increases in diversity enhance, rather than weaken, the stability of community dynamics, reversing the classic diversity-stability relation. Our results, based on mathematical analysis and simulations, are robust to a wide range of alternative assumptions and generalized modeling frameworks. We also find that the sublinear model is consistent with several well-known macroecological patterns, recovering production-biomass scaling across ecosystems, as well as the species abundance distribution, mean-variance scaling, and size-density scaling. As such, the model allows links to be drawn among distinct patterns of abundance. Finally, unlike the GLV model, but consistent with the biodiversity-ecosystem functioning literature, our model predicts that losses in biodiversity will tend to destabilize communities and lengthen their recovery time after disturbance.

**CONCLUSION:** The alarming rate of diversity loss means that ecology is in urgent need of a theoretical framework capable of making realistic predictions. We propose that the sublinear model is a viable description of population and community dynamics, drawing an intriguing parallel with individual growth dynamics. Population time series indicate that sublinear growth appears to be a more accurate model of population dynamics than the widely used logistic function. This small difference in the form of population growth allows collective regulation, reversing the theoretical diversity-stability relation predicted by decades of competition theory. Sublinear growth implies a positive diversity-stability relation, suggesting that diversity may be, in part, the cause of stability. Our results help to clarify the origin of the diversity-stability paradox, including the implicit assumptions in May's argument. Moreover, sublinear growth recovers common patterns of production, biomass, and abundance, offering a simple and general predictive framework. Although we still lack an understanding of the mechanistic origin of sublinear growth, our model is consistent with early ecological wisdom, modern macroecology, and what is known about some of Earth's most cherished ecosystems. ■

The list of author affiliations is available in the full article online.

\*Corresponding author. Email: [i.a.hatton@gmail.com](mailto:i.a.hatton@gmail.com)

†These authors contributed equally to this work.

Cite this article as I. A. Hatton *et al.*, *Science* **383**, eadg8488 (2024). DOI: [10.1126/science.eadg8488](https://doi.org/10.1126/science.eadg8488)

**S** READ THE FULL ARTICLE AT  
<https://doi.org/10.1126/science.adg8488>

## RESEARCH ARTICLE

## COMMUNITY ECOLOGY

# Diversity begets stability: Sublinear growth and competitive coexistence across ecosystems

Ian A. Hatton<sup>1,2,\*†</sup>, Onofrio Mazzarisi<sup>1,3,4,5†</sup>, Ada Altieri<sup>6</sup>, Matteo Smerlak<sup>1,7,8</sup>

The worldwide loss of species diversity brings urgency to understanding how diverse ecosystems maintain stability. Whereas early ecological ideas and classic observations suggested that stability increases with diversity, ecological theory makes the opposite prediction, leading to the long-standing “diversity-stability debate.” Here, we show that this puzzle can be resolved if growth scales as a sublinear power law with biomass (exponent  $<1$ ), exhibiting a form of population self-regulation analogous to models of individual ontogeny. We show that competitive interactions among populations with sublinear growth do not lead to exclusion, as occurs with logistic growth, but instead promote stability at higher diversity. Our model realigns theory with classic observations and predicts large-scale macroecological patterns. However, it makes an unsettling prediction: Biodiversity loss may accelerate the destabilization of ecosystems.

There is growing awareness that human activity is causing widespread species extinction, leading to a global biodiversity crisis (1–4). The effect that this has on the stability of ecosystems to continue to maintain function is not fully known, in large part because ecologists still struggle to understand the processes that naturally promote diversity and coexistence (5–12). Moreover, models typically fail to predict commonly observed large-scale patterns of production, biomass, and abundance (13–16), offering little hope that we might predict how stability and ecosystem properties are expected to change. Understanding these patterns and the dynamical processes that underlie them has long been at the heart of ecology and remains an urgent priority for global change research (4).

## The diversity-stability debate

The balance and stability of ecosystems was long thought to be related to their diversity (4, 7, 17–20). Early ecologists observed that pest outbreaks or large fluctuations in abundance are rare in diverse ecosystems such as tropical forests, whereas they are relatively com-

mon in simple systems, be they desert, arctic, or agricultural (4, 7, 17). More generally, they believed that the varied notions of ecological stability, which include the ability to recover from disturbance, to maintain a viable steady state and to buffer invasions, were enhanced by diversity (4, 7, 17–20). This conventional view stands in marked opposition to classic theories of competitive exclusion derived from the Lotka-Volterra competition model (21). This model combines logistic growth with mass-action interaction kinetics, whereby the competitive effect of a species on another varies as the product of their densities. The Lotka-Volterra model predicts that only one of two competing species can persist unless self-regulation is stronger than the competitive effect on growth. This model has since been generalized to any number of species (generalized Lotka-Volterra, GLV) and remains the most common model for studying competition, mechanisms of coexistence, and the diversity-stability relation (6, 8, 12, 22–26).

The GLV model has been shown to have very similar stability properties to those obtained from May’s general argument based on random matrix theory (5, 6, 12, 25). May showed that a system exhibits a sharp transition from stable to unstable interactions as it becomes more diverse (5, 6). Since then, many factors have been proposed that allow stability to be maintained as a system becomes more diverse (7, 8, 10, 11, 23, 27). These factors include more realistic parameter values (28), network structures (29, 30), and levels of connectance (31), as well as modularity (32, 33), hierarchy (34), and selection for stable interactions (35). There has also been renewed focus on the relative strength of self- versus cross-regulation (7, 8, 10, 36, 37), which is closely associated with resource partitioning (38) and niche differen-

tiation (8, 39). A great deal of work on food web interactions has emphasized the importance of structured random matrix systems (9), body size allometric constraints on interactions (40), and the covariance between interaction strengths (41). Finally, higher-order interactions can promote the stability of diverse systems, although pairwise interactions remain unstable (11, 42).

Although these factors are able to rescue stability at higher diversity, they have not been able to restore the conventional view that diversity is the parent of stability. Moreover, proposed mechanisms are not always general across different kinds of communities or large-scale gradients and typically fail to predict well-established empirical patterns [e.g., (13–16), but see (43–47)]. As such, ecology does not yet have a simple and general dynamical model that is consistent with the most common patterns of abundance and that recovers a positive diversity-stability relation. The purpose of this paper is to propose such a model.

## Sublinear population growth

Most prior dynamic ecological modeling has investigated the nature of the interactions between species, often by constraining the interaction matrix (5–7, 9–12, 23, 25, 28, 29, 41), with far fewer studies considering the population growth term. However, subtle differences in population dynamics can cause marked differences in community interactions (27).

Here, we contrast the logistic population growth model, classically used in GLV, with sublinear population growth. We call the model “sublinear” to align with the scaling literature. The model couples a sublinear growth term (biomass increases with an exponent  $k < 1$ ) and a linear loss term, in contrast to the logistic model that couples linear growth ( $k = 1$ ) and second-order loss (i.e., mass-action). The sublinear model of population growth is thus directly analogous to the Bertalanffy model of individual ontogenetic growth (48–51) but is not otherwise related to individual-level scaling.

The logistic and sublinear models can have a very similar sigmoid shape, and their fits to individual-level growth curves are often statistically indistinguishable (49, 52, 53), a problem that would also apply at the population level [see the supplementary materials, section S1 (54)]. However, the difference between these models becomes clearer when we consider the shape of the decline in per capita population growth with density, a hallmark of density dependence. This shape is linear under a logistic model, whereas it is concave-up in the sublinear model (resembling a curved “L”; Fig. 1A).

These models are both nested special cases of the more general  $\theta$ -logistic model (55, 56) [see the supplementary materials, section S1.1 (54)], which has been used to fit a diverse array of population time series (57–62). The fitted

<sup>1</sup>Max Planck Institute for Mathematics in the Sciences, 04103 Leipzig, Germany. <sup>2</sup>Department of Earth and Planetary Sciences, McGill University, Montreal, QC H3A 0E8, Canada. <sup>3</sup>Department of Ecology and Evolutionary Biology, University of Kansas, Lawrence, KS 66045, USA. <sup>4</sup>The Abdus Salam International Centre for Theoretical Physics (ICTP), 34014 Trieste, Italy. <sup>5</sup>National Institute of Oceanography and Applied Geophysics (OGS), 34014 Trieste, Italy. <sup>6</sup>Laboratoire Matière et Systèmes Complexes (MSC), Université Paris Cité CNRS, 75013 Paris, France. <sup>7</sup>Laboratoire de Biophysique et Evolution, UMR 8231 CBI, ESPCI Paris, PSL Research University, 75005 Paris, France. <sup>8</sup>Capital Fund Management, 75007 Paris, France.

\*Corresponding author. Email: i.a.hatton@gmail.com

†These authors contributed equally to this work.

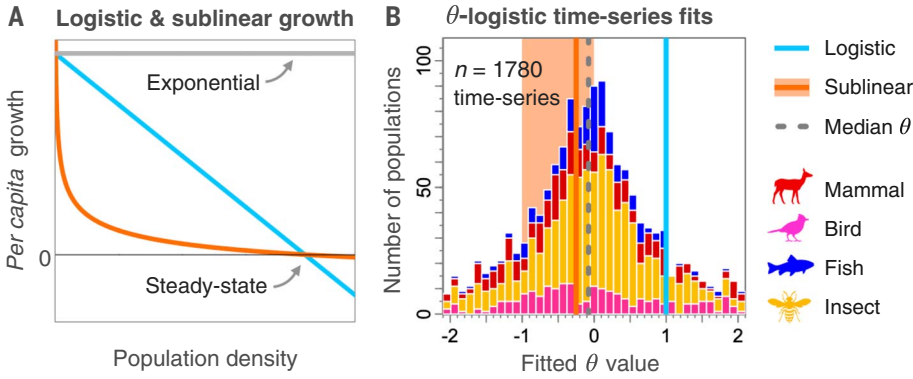


**Fig. 1. Logistic versus sublinear population growth.** (A) Both models can have similar time trajectories because their per capita growth is a decreasing function of population density, but whereas this function is linear for logistic growth (blue line), it is concave-up for sublinear growth (orange line). Both models are nested in the  $\theta$ -logistic model (see the materials and methods). (B) Summary of the analysis by Sibly *et al.* (57) showing maximum likelihood fits of the  $\theta$ -logistic model to their 1780 population time series across four major groups. Values of  $\theta$  near 1 (vertical blue line) indicate a logistic model, and values between  $-1 < \theta < 0$  indicate a sublinear model (orange shading from  $0 < k < 1$ ; vertical orange line is shown for reference at  $\theta = -0.25$ , equivalent to a sublinear exponent  $k = 0.75$ ). The median value of  $\theta$  for all populations is  $-0.08$ , corresponding to a weakly sublinear model (see the materials and methods).

value of  $\theta$  provides an empirical measure of the curvature in density dependence. An extensive analysis of 1780 population time series of mammals, birds, fish, and insects showed a strong tendency for concave-up relations between per capita growth rate and density (57). We show a slightly modified reanalysis of these time series that closely recovers the results reported in (57) (see the materials and methods and fig. S1). Representing these fitted  $\theta$  values in the context of the logistic and sublinear models lends support to the possibility that sublinear population growth may be a more realistic growth trajectory than logistic for many species [see Fig. 1B; the materials and methods; fig. S2; and the supplementary materials, section S1.5 (54)].

We find that the classic diversity-stability relation is reversed when sublinear population growth is embedded in a community model. For example, May concluded that communities of populations that are themselves stable become increasingly destabilized with the diversity of interactions (5) (Fig. 2A). By contrast, we find that communities of populations with sublinear growth, even those that are themselves unstable, become increasingly stabilized by diversity (Fig. 2B).

**Competition equations**

We model the dynamics of  $S$  species  $i$  with biomass densities  $B_i$  (mass per unit area) as

$$\frac{dB_i}{dt} = P_i(B_i) + C_i(B_1, \dots, B_S) \quad (1)$$

where  $P_i$  is a growth function representing intraspecific density dependence (population-level) and  $C_i$  captures the effect of interspecific

interactions (community-level). We consider two forms of population density dependence:

$$P_i(B_i) = \begin{cases} (r_i - z_i)B_i(1 - B_i/K) & \text{(logistic)} \\ r_i B_0^{1-k} B_i^k - z_i B_i & \text{(sublinear)} \end{cases} \quad (2)$$

Each model has three parameters: the physiologically constrained birth rate  $r_i$  and death rate  $z_i$  of a species  $i$  and a constant with units of biomass density: the logistic carrying capacity  $K$ , and the sublinear model constant  $B_0$ . While  $K$  is usually interpreted as the maximum biomass density achievable by a population, the constant  $B_0$  can be viewed as a lower bound on biomass density, corresponding to the maximum per capita growth rate  $P_i/B_i \approx r_i$ . We consider the exponent  $k < 1$  as a constant across all species, as in the individual-level Bertalanffy model (48–50), and use  $k = 3/4$  as a reference value for the purposes of presentation. We emphasize, however, that a broad range of values in  $0 < k < 1$  leads to the same qualitative outcomes.

To align with the GLV model and prior theory, we retain the common mass-action assumption for species interactions:

$$C_i(B_1, \dots, B_S) = -\sum_{j \neq i} A_{ij} B_i B_j \quad (3)$$

Combined with logistic growth (Eq. 2), this assumption (Eq. 3) defines the classic GLV model (see the materials and methods). The sign and value of the coefficients  $A_{ij}$  characterize the type and strength of interaction between species. This assumption may be questionable in the context of predation or mutualistic interactions because in these cases,

growth rates may exceed the maximum physiological limit to birth rate,  $r$ , due to the added effect of positive interactions. For competitive interactions (corresponding to  $A_{ij} > 0$ ), however, this assumption only acts as an additional loss term. Here, we contrast logistic growth with an extreme form of the sublinear model where natural death rates  $z_i = 0$ , such that populations are themselves unstable because any positive death rate only enhances stability. As a null model, we assume no special structure for the interaction network: Each interaction  $A_{ij}$  is drawn from a common distribution with mean  $\mu$  and SD  $\sigma$ . We also show that this assumption could additionally apply to populations growing sublinearly [see the supplementary materials, section S5.1 (54)]. Further, we consider alternatives to mass-action community competition (63) and investigate the interaction term generalized to a broader class of community dynamics [see the supplementary materials, section S6 (54)].

**Results**

Because populations under logistic growth are individually stable and collectively unstable, we might expect that populations under sublinear growth that are individually unstable (when  $z_i = 0$ ) are even less likely to be collectively stable. We now show that the opposite is true.

**Collective competitive coexistence**

For simplicity, first consider all species couplings as competitive with the same interaction strength ( $A = \mu > 0$ ,  $\sigma = 0$ ). For a community to be locally stable in both models, per capita production  $p_i = P_i/B$  and competition  $c_i = C_i/B$  must satisfy the condition for a multispecies equilibrium  $\mathbf{B}^*$  [see the materials and methods and the supplementary materials, section S2 (54)]:

$$\left| \frac{\partial p_i}{\partial B_i} \right| > \left| \frac{\partial c_i}{\partial B_j} \right| \quad (4)$$

This inequality shows that stability is only possible if the interactions of a species with itself (LHS) are more strongly density dependent than its interactions with other species (RHS) on a per capita basis. Within the GLV, this inequality translates into the condition that  $r/K > \mu$ , which means that population interactions must be stronger than community interactions. However, in the sublinear model, Eq. 4 leads to a very different condition that depends on diversity  $S$  and the sublinear exponent  $k$  [see the materials and methods and the supplementary materials, section S2 (54)],

$$S > 1 + \frac{1}{1 - k} \quad (5)$$

That is, under sublinear growth, local stability is (i) possible in the absence of individual population stability, (ii) independent of the

individual growth rate or the strength of competition, and (iii) enhanced by greater species richness (i.e., a larger  $S$  implies a faster return to equilibrium). This argument uses  $z_i = 0$ , but any positive level of mortality  $z_i$  in the model

only serves to augment system stability [see the materials and methods and the supplementary materials, section S2 (54)].

These results generalize to random competitive interactions, where each  $A_{ij}$  is an inde-

pendent random variable with positive mean  $\mu$  (corresponding to competitive coupling) and SD  $\sigma$ . Figure 3 shows three alternate depictions of the opposing stability properties of logistic and sublinear growth models [see the materials and methods and the supplementary materials, section S3 (54)]. In Fig. 3, A and B, we choose a single set of parameters and interaction statistics ( $\mu, \sigma$ ) to show that stable coexistence decreases with diversity for GLV with logistic growth, but increases with sublinear growth. These opposing stability properties can be demonstrated across different values of  $\mu$  and  $\sigma$  of the interaction matrix  $A_{ij}$ . Following convention (24), we consider diversity-weighted values of these parameters ( $\mu\sqrt{S}$  versus  $\sigma\sqrt{S}$ ; Fig. 3C) such that for a given positive  $\mu$  and  $\sigma$ , increasing diversity follows a square root law upward from the origin. The differing stability boundaries of logistic and sublinear growth models show that increasing diversity moves a system out of the stable regime of logistic growth and into the stable regime of sublinear growth (see also fig. S4). Finally, we report replica calculations to provide exact results for symmetric interactions of very large systems under logistic and sublinear growth, which offer an alternate view of a similar conclusion [see the materials and methods; fig. S7; and the supplementary materials, section S4 (54)]. Analyses and simulations of sublinear growth scaling thus paint a picture of the complexity-stability relationship that is opposed to the principle that large, tightly coupled communities must be unstable.

Up to now, we have assumed that there is no lower bound on biomass density, which in many cases is unrealistic. For example, a minimum density could arise in which the rate of encountering a mate falls below mortality rate.

**Fig. 2. Time-trajectories of single versus multispecies logistic and sub-linear growth models.** All models are shown comprising the same rates of growth  $r$  and mortality  $z$ , and all plots have the same scale (parameter values are listed in the materials and methods).

(A and B) Single-species logistic growth (A) and sublinear growth ( $k < 1$ ) (B) population models (top row) have different forms of density dependence that both lead to a stable single-species equilibrium in biomass  $B$  but have differing behavior in a multispecies competitive community model (bottom row). With increasing species diversity, logistic growth leads to increasing instability, whereas sublinear growth leads to increasing stability. The positive diversity-stability relation of the sublinear growth model holds even in the unrealistic case when individual populations are themselves unstable ( $z = 0$ ; not shown).

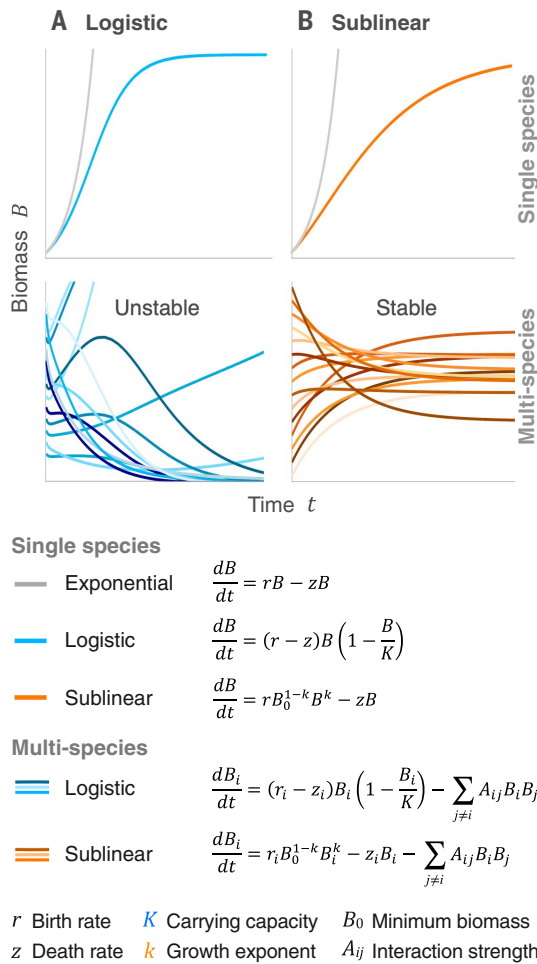
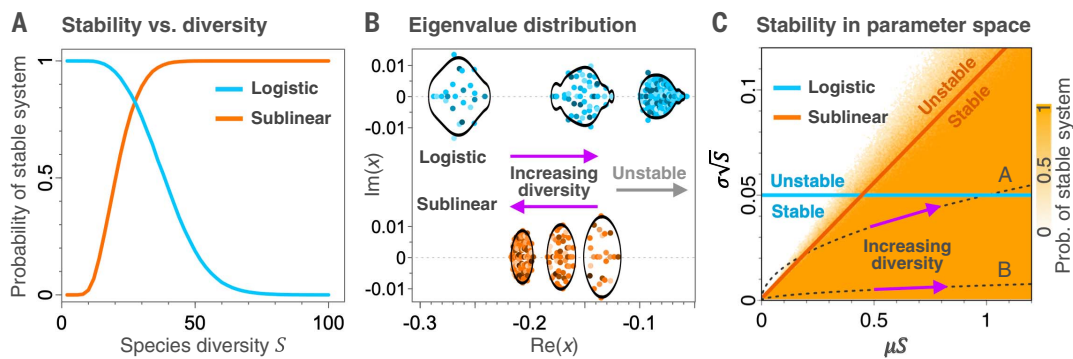


**Fig. 3. Contrasting diversity-stability relations for logistic and sublinear growth.** We set model parameters the same across all plots (listed in the materials and methods) and vary the species richness  $S$  for a given mean  $\mu$  and SD  $\sigma$  of the interaction matrix  $A_{ij}$ .

(A) With increasing  $S$ , the probability of obtaining a stable system declines to zero under logistic growth but increases to one under sublinear growth. (B) The distribution of eigenvalues of the community matrix are shown in the complex plane.  $Re(x)$  and  $Im(x)$  denote the real and imaginary axes, respectively. Increasing diversity under logistic growth pushes eigenvalues closer to the instability threshold at zero, whereas under sublinear growth, eigenvalues are pushed away from zero (shown at three diversity levels). Black lines encircling eigenvalues are computed from equilibrium biomasses using results of (93). (C) The stability phase diagram for both models generalizes these results over positive values of  $\mu$  and  $\sigma$ , here shown scaled by diversity for



large  $S$  ( $\mu\sqrt{S}$  and  $\sigma\sqrt{S}$ ). Increases in diversity trace a square root curve for a given  $\mu$  and  $\sigma$ , shown here as dashed black lines for  $\mu$  and  $\sigma$  values from plots (A) and (B). The orange line is the analytical critical stability threshold, and color shading shows sublinear model simulations. Logistic growth stability resides below a horizontal threshold, whereas sublinear growth stability resides below a linearly increasing function, whose slope depends in part on the sublinear growth exponent,  $k$  [see the materials and methods and the supplementary materials, section S3.2 (54)].

Assuming that extinction occurs at  $B_0$  places an upper bound on diversity and interaction strength. In more diverse and tightly coupled communities, the biomasses of all species are suppressed, eventually triggering extinction when a species reaches this threshold and making the equilibrium unfeasible [see the supplementary materials, section S3.3 (54)]. In the sublinear model, a lower limit on density implies that there are upper limits to diversity and interaction strength. Nonetheless, within these limits, diversity maintains a positive relation to stability (figs. S6 and S11).

We have tested the robustness of our findings to a wide range of alternative assumptions [see the supplementary materials, section S5 (54)], including different behaviors below the biomass threshold  $B_0$  (fig. S10), varying levels of connectance or possible structure such as modularity in  $A_{ij}$ . We have also investigated explicit consumer-resource frameworks [see figs. S11 to S13 and the supplementary materials, section S5.5 (54)]. Furthermore, we have generalized the findings presented above in several ways, including positive levels of mortality [ $z > 0$ ; see figs. S3, S4, and S6 and the supplementary materials, section S3 (54)], second-order population interactions [see figs. S8 and S9 and the supplementary materials, section S5.1 (54)], and alternative scaling in community interactions beyond simple mass-action [see the supplementary materials, section S6 (54)]. In all of these cases, our results are robust: Sublinear growth means that diversity begets stability.

### Macroecology predictions

The sublinear model provides realistic predictions for a variety of macroecological patterns. This model was previously proposed to account for predator versus prey biomass scaling across clearly delineated trophic communities (64), as well as omnivorous food webs (65). Closely related is the pattern of production-biomass scaling across ecosystems (Fig. 4). Each point in Fig. 4 represents a separate ecosystem, whereas each regression encompasses a distinct community type, such as large mammals, invertebrates, fish, and plankton, across a large gradient in biomass (64) (figs. S14 and S15 and table S2). Production represents the maximum total change in biomass density in a population or community over a period of time, which could be a productive season of the year or the duration of an experiment. Biomass exponent values are usually significantly sublinear ( $k < 1$ ), with best fits often ranging from  $k = 2/3$  to  $k = 3/4$ , with piscivorous fish as the only major outlier (64) (see the materials and methods, figs. S14 and S15, and table S2).

To model these patterns, we consider each point in Fig. 4 a community near equilibrium and assume a common value for all species of

$k = 0.75$  and  $B_0 = 0.01$  g/m<sup>2</sup>. We parameterized  $r$  and  $z$  from independent data for each major community type (Fig. 5A) while varying  $\mu$  and  $\sigma$  by a common factor across a community gradient. These assumptions allow the overall relation to be recovered, including the slope (by assumption) and both the intercept and biomass range, from individual-level growth and mortality rates [see Fig. 5B; the materials and methods; and the supplementary materials, section S7 (54)].

Unexpectedly, this same set of assumptions also makes realistic predictions for other well-known patterns in macroecology, including the species abundance distribution (13, 66), mean-variance scaling [Taylor's law (14)], size-density scaling [Damuth's law (15, 16, 67)], and possibly the size spectrum [the Sheldon spectrum (68, 69)]. We found that representative empirical examples of each of these patterns are closely matched to corresponding model predictions (see the materials and methods). Not only is the model consistent with the overall form of these patterns, but in some cases makes reasonable predictions for the slope, intercept, and residual variation (see the materials and methods). Although prior theory has shown how some of these patterns can be predicted (43, 44, 46, 47, 70), we are not aware of a model capable of predicting cross-

system dynamics (Fig. 4) and different aspects of abundance with the same set of simple assumptions [see the supplementary materials, section S8 (54)].

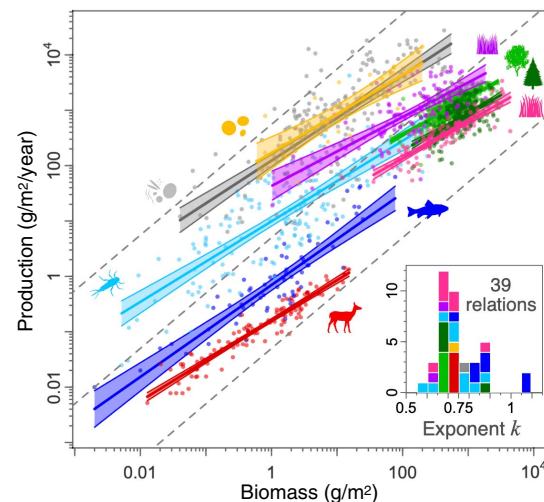
For the logistic growth model to recover these patterns, one requires  $r \sim K^{-1/4}$ , an additional assumption that is difficult to justify [see fig. S17 and the supplementary materials, section S9 (54)]. Not only does this assumption remove a free parameter and constrain model flexibility for fitting population time series, but the needed relation between  $r$  and  $K$  is distinctly at odds with well-known body mass allometry [see the supplementary materials, section S9.5 (54)]. Moreover, given that the GLV model is not inherently stable, especially at high diversity (Fig. 3), unstable interactions must be filtered out or weakened to ensure community coexistence across these large-scale gradients. We therefore consider the sublinear growth model to be more parsimonious and realistic than logistic growth for modeling large-scale abundance patterns [see the supplementary materials, section S9.5 (54)].

### Discussion

We propose that population growth may scale as a sublinear power law with biomass. Not only is sublinear population density dependence

**Fig. 4. Sublinear growth scaling with biomass across ecosystems.** For a given community type across  $n$  separate ecosystems, the log of total community productivity is regressed against the log of biomass, with the ordinary least squares fitted exponent and 95% confidence interval exhibiting values of  $k < 1$ . The dashed gray lines show linear production ( $k = 1$ ), implying a constant reproduction rate regardless of density. The inset shows a histogram of  $k$  values for these and additional regressions that derive from additional sources or different subsets of the aggregated data shown based on individual published meta-analyses.

The outlier with a superlinear exponent ( $k > 1$ ) is for piscivorous lake fish ( $n = 30$ ). See also figs. S14 and S15 and table S2.



Community type	$n$	$k$	(95% C.I.):
Large mammals	118	<b>0.73</b>	(0.69 - 0.77)
Phytoplankton	24	<b>0.70</b>	(0.48 - 0.93)
Broadleaf trees	592	<b>0.66</b>	(0.62 - 0.71)
Coniferous trees	384	<b>0.66</b>	(0.58 - 0.76)
Invertebrates	164	<b>0.73</b>	(0.64 - 0.81)
Freshwater fish	70	<b>0.83</b>	(0.72 - 0.94)
Seagrass beds	105	<b>0.62</b>	(0.50 - 0.74)
Grasslands	95	<b>0.67</b>	(0.60 - 0.75)
Marine bacteria	207	<b>0.77</b>	(0.68 - 0.86)

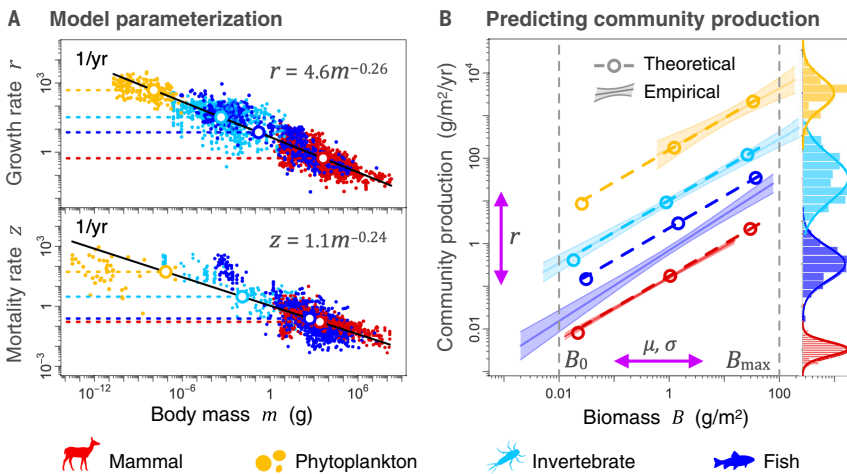


**Fig. 5. Modeling production-biomass relations.** The sublinear model can be parameterized to yield predictions for production-biomass relations in Fig. 4, shown here for mammals, phytoplankton, invertebrates, and fish. **(A)** Parameters of  $r$  and  $z$  for each community type are obtained from the geometric mean of all available data (15) for each group. **(B)** To simulate the regressions of the four groups in Fig. 4, we make the following additional assumptions:  $k = 3/4$  (from Fig. 4),  $S = 50$  (arbitrary),  $\sigma/\mu = 1$  (arbitrary), and  $B_0 = 0.01 \text{ g/m}^2$  for all groups (from Fig. 4). We also make the simplifying assumption that  $z = r/10$ , given that values are often near this estimate (see the materials and methods). To increase biomass  $B^*$  along a gradient, we decrease both  $\mu$  and  $\sigma$  by a common factor. The model recovers the slope (by assumption,  $k = 3/4$ ), intercept ( $rB_0^{1-k}$ ), and biomass range [ $B_0$  to  $B_{\max} = B_0(z/r)^{1/k}$ ] of the production regressions (empirical confidence intervals are shown as shaded colored regions in the plot). The residual variation of each empirical regression is shown on the RHS on the same scale as production and later used to predict the species abundance distribution (see the materials and methods).

consistent with extensive time-series data (57) (Fig. 1B), but the sublinear community model is more parsimonious and realistic than the logistic for modeling several macroecological patterns (see Fig. 5 and the materials and methods). But why should sublinear population growth have such an opposing collective effect on community stability from what classic theory predicts?

The common rule of thumb that stability requires population interactions to be stronger than community interactions is subtle. Stability lies not in their relative strength per se, but in their relative rates of change, as measured by the elements of the community matrix (10). This means that even very many strong interactions need not destabilize a community if population interactions change faster than community interactions (Eq. 4). This can be readily seen by considering a generalization of our modeling framework, which permits alternative scaling in community interactions beyond simple mass action [see the supplementary materials, section S6 (54)]. Calculations of the stability properties of this more general model reveal that the regime in which “diversity begets stability” is conserved for a broad class of dynamics as long as population growth scaling is less than the scaling of population loss from community interactions [see the supplementary materials, section S6 (54)].

The GLV model corresponds to the boundary of this regime when all competitive interactions are of equal strength ( $\sigma = 0$ ), but any variation in competitive coupling ( $\sigma > 0$ ) quickly enters the regime where diversity is destabilizing [see the supplementary materials, section S6 (54)]. These results imply that the diversity-stability relation depends on the relative density dependence between population and community interactions [see the supplementary materials, section S6 (54)], offering a more nuanced but comprehensive view of the diversity-stability relation.

The theoretical diversity-stability relation stems from the interplay of population interactions with community interactions, specifically the dependence of community matrix elements on diversity. May’s argument assumed that community matrix elements, including diagonal elements, are independent of diversity  $S$  (5, 6). This assumption effectively holds under logistic growth but not under sublinear growth, where diagonal and off-diagonal elements of the community matrix scale differently with  $S$  through their dependence on equilibrium biomass  $B^*$  [see the supplementary materials, section S3 (54)]. This difference in the scaling with diversity in the sublinear model means that increases in diversity result in a more negative real part of the largest eigenvalue. Contrary to May’s result, the sub-

linear model thus predicts that more diverse communities should be more resilient and lead to shorter damping time [equivalent to the inverse of the magnitude of the largest eigenvalue (71)].

The implication of these findings is that species losses in disturbed ecosystems may further destabilize communities and slow their recovery after disturbance. This prediction has crucial applied relevance amidst global declines in biodiversity and appears to be gaining observational support. Recent reviews of the biodiversity-ecosystem functioning relation have shown that more diverse systems often recover more rapidly from disturbance (72–75), though with some notable exceptions [see the supplementary materials, section S12 (54)].

### Limitations

The connections of our modeling framework to empirical observations are limited by data quality. We have attempted to link the model to time-series data, based on model fitting (Fig. 1B) (57–62), and to production-biomass and abundance patterns, based on model predictions (Fig. 4 and 5). Although the time-series data are extensive (the full dataset includes almost 180,000 population census observations across 720 species; see the materials and methods), many of these time series are very short, vary over a limited range of abundance, and are measured in the presence of other species with whom the focal population may interact. As a result, our fits of the  $\theta$ -logistic growth model sometimes revealed unrealistic parameter values. We thus hesitate to draw strong inference from time-series analysis until high-quality data can unequivocally distinguish the sublinear model from other functional forms [see the supplementary materials, section S1 (54)]. Similarly, many of the production-biomass relations (Fig. 4) and abundance patterns (see the materials and methods) are compiled from different sources, each with different aims and methods. Although the sublinear model makes realistic predictions of these macroecological patterns, avoiding the  $r$  versus  $K$  dependence needed by the GLV model [see the supplementary materials, section S9.5 (54)], further research is needed to improve the scope and number of these relations across new community types.

We also lack a good understanding of the origin of sublinear growth dynamics (53, 64). Nonetheless, certain animal behaviors and geometric constraints may offer clues as to possible kinds of relevant processes. In mammals, for example, group size often exhibits sublinear scaling with population biomass (76, 77) (fig. S3). Group-size scaling should result in sublinear population growth scaling if a limited number of individuals monopolize reproduction in a group, such as the parents of a family or a dominance hierarchy that promotes

reproductive skew (78) [see the supplementary materials, section S11.2 (54)]. Coupling such a population process with competition for an additional resource that is depleted in proportion to the densities of all other species would allow us to link these processes to the terms of our model. Alternatively, there may exist a surface-volume constraint such as that thought to underlie the widely observed self-thinning rule in forest stands (79). This form of sublinear density dependence could be associated with growth scaling of all trees near  $\frac{3}{4}$ , but it remains less clear how to connect such a process to our model without possibly additional considerations [see the supplementary materials, section S11.3 (54)]. Finally, some of the many factors that give rise to negative frequency dependence (10), including those thought to ultimately underlie stability and coexistence (7, 8, 10, 11, 28), may more proximally underlie sublinear growth. Given the specific reproductive and grouping behaviors of species, we should not expect density dependence at population and community levels to be equivalent, but why growth scaling may be sublinear remains unresolved [see the supplementary materials, section S11 (54)].

Of course, we have only considered competitive interactions under sublinear growth, which allowed us to draw general conclusions about one class of interactions but neglects the many and varied food web, mutualistic, and parasitic interactions that are still needed for a more complete understanding of ecosystem dynamics. Although we considered two consumer resource frameworks to explore competition for a shared resource under sublinear growth [see figs. S12 to S14 and the supplementary materials, section S5.5 (54)], these models can also be used to study other kinds of interactions such as cross-feeding, in which by-products from one species serve as resources for another (80).

#### Links to lower levels

Many of these same limitations have notable parallels at the individual level of organization. Growth at the individual level, be it prenatal, ontogenetic or reproductive (Fig. 5A) is well known to scale near  $\frac{3}{4}$  with body mass across species (15, 67, 81–83), similar to the way that population and community production scales with biomass across ecosystems (64) (Fig. 4). Individual ontogenetic growth curve data, however, are often unable to distinguish among alternative sigmoid models such as the logistic and sublinear Bertalanffy models (49, 52, 53). This is perhaps surprising given these individual-level data are of high quality, span a broad range of values, and are measured in the absence of possibly confounding factors [see the supplementary materials, section S1.2 (54)]. Moreover, the link between the cross-species patterns (maximum growth

versus adult body mass) and the dynamic model (e.g., Bertalanffy) describing the growth of an individual is often tenuous and taken for granted at the individual level (48–51, 67). At both levels of organization, further work is needed to more explicitly connect the cross-system pattern with the within-system dynamics.

Despite the much longer history of body mass scaling, there is also still little consensus on the underlying processes responsible for these patterns or dynamics (15, 49, 84). Growth scaling is often explained in terms of metabolic scaling (50, 51, 67, 85), the origins of which are still widely debated, and there is growing evidence that body mass scaling allometries may be better understood as originating with growth itself (15, 49, 84). Given the recurrent similarities in growth scaling across levels of organization, it is possible that the same kind of abstract dynamical processes are responsible for sublinear growth at both the individual and population levels (15, 53).

These individual-level limitations, however, have not hindered body mass scaling relations from being used to make predictions, which rank as some of the most general and robust in ecology (15, 67, 83). Our model makes use of individual-level data (see Fig. 5 and the materials and methods) to give realistic quantitative predictions and suggest connections among common patterns of production, biomass, and abundance. Moreover, the sublinear model qualitatively aligns theory with ecological intuition about the role of diversity in maintaining stability, as well as results from biodiversity-ecosystem functioning research (72–75) [see the supplementary materials, section S12 (54)]. This modeling framework may offer holistic estimates of ecological properties, which holds promise for identifying critical thresholds in disturbance regimes or for forecasting changes in ecological function with changes in biodiversity.

#### Conclusions

Ecologists have long puzzled over the source of the enduring stability of complex ecosystems. Our results show that sublinear growth scaling is intrinsically stabilizing as the diversity of competitive interactions increases. These results revive conventional wisdom that stability is conditioned on diversity rather than a mere possibility under the right circumstances. Our model offers compelling prospects for linking dynamical theory with macroecology, highlighting links between distinct patterns in dynamics and abundance. It also predicts that biodiversity loss may lengthen recovery time after disturbance and increase the likelihood of destabilization. Although we have yet to uncover how sublinear growth mass scaling can emerge, a sublinear growth model offers a framework that may yield better pre-

dictions for nature's balance and patterns of abundance.

#### Materials and methods

Our methods are summarized below and described further in the supplementary text and the additional figures and tables in the supplementary materials. All data and sources are provided in data S1 [listed in tables S3 and S4, and further described in the supplementary materials, section S10 (54)]. All code reproducing our analyses is available at <https://zenodo.org/doi/10.5281/zenodo.10476101>.

#### Time-series support for sublinear growth

Prior work has shown that many populations in nature exhibit concave-up curvature in population density dependence (57–62). This has been demonstrated by fitting time series to the  $\theta$ -logistic model (55, 56), where the value of  $\theta$  allows flexibility in the curvature of density dependence, including concave-down ( $\theta > 1$ ), linear (logistic growth;  $\theta = 1$ ), and concave-up ( $\theta < 1$ ). Special cases of the concave-up  $\theta$ -logistic include the Gompertz model ( $\theta = 0$ ) (86, 87) and a model for immigration ( $\theta = -1$ ), the latter of which has been shown to be broadly stabilizing (88, 89). Between these values resides the sublinear model ( $-1 < \theta < 0$ ) [see the supplementary materials, section S1.1 (54)].

The  $\theta$ -logistic model has been criticized for population time-series fitting, given that fitted maximum growth rates  $r$  show an inverse dependence with fitted values of  $\theta$  (90). This problem is largely overcome by introducing a new growth-related positive parameter  $\alpha$  and scaling the  $\theta$ -logistic model by the inverse of  $\theta$ :

$$\frac{dB}{dt} = \frac{\alpha}{\theta} B \left( 1 - \left( \frac{B}{K} \right)^\theta \right) \quad (M.1)$$

allowing a smooth transition to negative  $\theta$  values through zero and easily recovering other nested models [see the supplementary materials, section S1.1 (54)]. Here,  $B$  is the population density of a species. In the logistic growth case ( $\theta = 1$ ),  $\alpha \equiv r - z$ , whereas in the sublinear growth case ( $-1 < \theta < 0$ ),  $\alpha/|\theta| \equiv z$ , and  $K^{-\theta}\alpha/|\theta| \equiv rB_0^{-\theta}$  [see the supplementary materials, section S1.1 (54)]. These modifications allow parameters  $\alpha$  and  $\theta$  to be fit largely independently of one another (fig. S1A) while easily allowing the recovery of nested models (table S1).

To summarize the results of the Sibly *et al.* analysis (57) in the context of logistic and sublinear population growth models, we made use of this adaptation to the  $\theta$ -logistic model and reanalyzed their original data. All data derive from the Global Population Dynamics Database (91, 92), which includes 4471 population time series (179,859 census observations) from which Sibly *et al.* (57) selected 1780 on the basis of several criteria across

the four major taxonomic groups of mammals, birds, fish, and insects (36,495 census observations).

Following methods in (90), we maximize the log-likelihood function given the parameters  $\alpha$ ,  $K$ ,  $\theta$ , and  $\sigma$ . For each transition in observed population abundance  $B_t \rightarrow B_{t+1}$ , we calculate  $\log_e(B_{t+1}/B_t)$  and minimize the difference with modeled per capita growth transitions  $\frac{\sigma}{\theta} \left(1 - (B/K)^\theta\right)$ . We evaluate the likelihood of each transition for a given set of parameters using numerical optimization provided by the Matlab functions in (90). Despite the differences in our analysis, including our formulation of the  $\theta$ -logistic model and our fitting routine, we obtain very similar  $\theta$  values to those reported in Sibly *et al.* (57) [see fig. S1B and the supplementary materials, section S1.5 (54)].

Fitted  $\theta$  values show a single-peaked frequency distribution across 1780 populations of mammals ( $n = 374$ ), birds ( $n = 302$ ), fish ( $n = 228$ ), and insects ( $n = 876$ ), closely reproducing the results of (57) and shown in Fig. 1B. Fits exhibit wide variation in  $\theta$  values, however, often exceeding  $\pm 10$  (SD is 6.9). We avoid representing these unrealistic values by only representing the distribution of  $\theta$  over  $[-2, 2]$ . Given this wide variation, we consider the median value of  $\theta$  as a measure of central tendency.

The distribution of fitted  $\theta$  values in Fig. 1B are notably shifted below  $\theta = 1$ , representing concave-up density dependence, as reported by Sibly *et al.* (57). These values frequently fall in the sublinear domain,  $-1 < \theta < 0$ , with far fewer time series having  $\theta \approx 1$  (logistic). The median value of all 1780 population time series is  $-0.08$ , corresponding to a weakly sublinear central tendency (Fig. 1B). Very similar distributions of  $\theta$  values are obtained using the  $\theta$ -scaled  $\theta$ -logistic over the full GPDD of  $n = 4168$  time series, as well as a stricter set of selection criteria than used by Sibly *et al.* (57) from (90), resulting in  $n = 364$  time series (fig. S2). Although values of  $\theta = 0$  (Gompertz model) also appear realistic, the sublinear model more generally encompasses a larger number of populations, and we restrict our analysis to contrasting logistic with sublinear growth [but see the supplementary materials, section S2, for the stability characteristics of other nested  $\theta$ -logistic models (54)]. As we report [see the supplementary materials, section S1.5 (54)], all median  $\theta$  values under all selection criteria and within all major taxonomic groups are within the domain of the sublinear model.

We take these findings as suggestive that sublinear growth is a likely description of population dynamics and a viable alternative to logistic growth at the community level. A more conclusive analysis, however, may require high-quality time series that span a large range in abundance, including very low densities,

over many generations, and in the absence of other confounding factors. Such datasets are difficult to obtain from natural systems and may require controlled density-growth experiments over a range of taxa.

### Community model setup

The GLV model has traditionally considered the dynamics of  $S$  interacting species in terms of their numerical abundance  $N$ . We cast the community model in terms of biomass density,  $B$ , which permits closer connections to empirical data (Fig. 4) and allows species of very different body masses to interact at more even interaction strengths. Both models are mathematically equivalent given average species body mass  $m$  ( $B = mN$ ).

Birth and death rates have the same meaning in both logistic and sublinear growth models ( $r$  and  $z$  have units of 1/time). In the logistic model, however, death rate can be subtracted from birth rate to obtain a new exponential growth rate ( $r - z$ ), which is not the case in the sublinear growth model. The distribution of the values in the interaction matrix  $A_{ij}$  is Gaussian for our analytical treatment to align with prior theory but is gamma distributed to ensure positive (competitive) interactions when we test the model against macroecological data (see Fig. 5 and the subsection “Modeling abundance data” below). Similarly, we present our theoretical results in the absence of mortality ( $z = 0$ ) because it represents the extreme case where populations are not individually stable and  $z > 0$  acts only to enhance stability. Our theoretical analysis presented in the supplementary materials (54), however, accounts for positive values of mortality  $z > 0$  [see the supplementary materials, section S3, and Eq. M.8 in the materials and methods (54)]. For testing the model against empirical data, we also assume  $z > 0$ , setting both  $r$  and  $z$  from auxiliary data (Fig. 5A).

We refer to power law growth with exponent  $k < 1$  as sublinear to align our terminology with the biological scaling literature, although logistic growth can also be considered a form of sublinear growth with biomass. The per capita growth relation with density, shown in Fig. 1A, presents a more distinctive sense of the term “sublinear” with respect to logistic.

### Stability criteria for uniform interactions

For uniform interactions ( $\sigma = 0$ ), the stability of a multispecies equilibrium  $B^*$  with respect to small perturbations of biomasses is determined by the spectrum of the community matrix  $J^*$ , defined as the Jacobian of the system evaluated at that equilibrium point. The equilibrium is (linearly) stable if and only if the dominant eigenvalue  $\lambda$  of  $J^*$  has negative real part. In the special case in which all species have equal growth rate  $r$  and all interactions have equal strength  $\mu$  (and thus all

equilibrium biomasses are equal), the community matrix has equal diagonal elements

$$J_{ii}^* = B^* \frac{\partial p_i}{\partial B_i} \quad (M.2)$$

and equal off-diagonal elements

$$J_{ij}^* = B^* \frac{\partial c_i}{\partial B_j} \quad (M.3)$$

(both negative if per capita growth decreases with density), and we have

$$\lambda = B^* \left( \frac{\partial p_i}{\partial B_i} - \frac{\partial c_i}{\partial B_j} \right) \quad (M.4)$$

The linear stability condition is therefore

$$\left| \frac{\partial p_i}{\partial B_i} \right| > \left| \frac{\partial c_i}{\partial B_j} \right| \quad (M.5)$$

We now contrast the implication of this condition in the logistic and sublinear growth models, for which  $\partial c_i / \partial B_j = -\mu$ , but diagonal coefficients differ. In the logistic growth model, where  $p_i = r(1 - B/K)$ , we have  $\partial p_i / \partial B_i = -r/K$ , so the linear stability condition translates into

$$r/K > \mu \quad (M.6)$$

a classic condition relating population and community interaction coefficients. In the sublinear model, in the extreme case of negligible mortality,  $z = 0$ , we have instead  $\partial p_i / \partial B_i = (k - 1)p_i(B^*)/B^*$ . Because  $p_i(B^*) = c_i(B^*) = (S - 1)\mu B^*$  at equilibrium, we get  $\partial p_i / \partial B_i = (k - 1)(S - 1)\mu$ , and the condition becomes  $\mu < (k - 1)(S - 1)\mu$ , i.e.

$$S > 1 + 1/(1 - k) \quad (M.7)$$

independently of  $r$  and  $\mu$ . Linear stability in the sublinear model therefore places a lower bound on species richness  $S$  but no restriction on growth rate or interaction strength. When  $z > 0$ , this condition is sufficient but not necessary for local stability [see the supplementary materials, section S2 (54)].

### Analytical solution for population biomasses

The cavity method is a standard technique in the physics of disordered systems that was first applied to the GLV model by Bunin (24). We use it here to estimate the distribution of equilibrium biomasses in the presence of random interactions  $A_{ij}$  with mean  $\mu > 0$  and SD  $\sigma$ ; we also assume that individual growth rates  $r_i$  and mortalities  $z_i$  are drawn independently from a distribution. Under these conditions, the cavity solution of the sublinear growth model is the random variable

$$B^* = B_0 \left[ \left( z + \mu SE_1^* + \sigma \sqrt{SE_2^*} \eta \right) / r \right]^{1/(k-1)} \quad (M.8)$$

where  $\eta$  is a standard normal variable and  $E_1^*$  and  $E_2^*$  are the first and second moments of  $B^*$ ,

respectively. This approximation closely aligns with simulations, as shown in fig. S3. The corresponding density function, equivalent to the species abundance distribution (see below), can be computed self-consistently from this equation, as detailed in supplementary materials, section S3.1 (54).

**Stability criteria for random interactions**

Once we know the equilibrium species abundance distribution, it is possible to estimate the distribution of eigenvalues of the community matrix in the complex plane. Ahmadian *et al.* (93) consider large, partially random matrices of the form  $M + LJR$ , where  $M$ ,  $L$ , and  $R$  are deterministic matrices and  $J$  is a random matrix with coefficients that are sampled independently from a distribution with mean zero and variance  $\sigma^2$ . Generalizing the famous “circular law,” which is the foundation of May’s original argument, they derive a condition for all eigenvalues to have negative real part. Applying this condition to the community matrix in the GLV, we find that all eigenvalues have negative real part provided  $\sigma S + \mu < r/K$ , as per May’s instability threshold (5, 12). In the sublinear model, however, we obtain instead the stability condition

$$\sum_i \left[ \mu - (1 - k)(B_i^*)^{k-2} \right]^{-2} < \sigma^{-2} \quad (M.9)$$

Combining this condition with the cavity solution for  $B^*$  allows us to compute the boundary of the stable phase in the  $(\mu, \sigma)$  plane, shown as the orange line in Fig. 3C. Further information is available in supplementary materials, section S3 (54).

In the special case where interaction coefficients are symmetric ( $A_{ij} = A_{ji}$ ), we can use an alternative approach to disordered systems known as the “replica formalism” [see the supplementary materials, section S4 (54)]. Applied to community ecology, this method consists in mapping the dynamical system to a disordered system at thermal equilibrium with Hamiltonian

$$\mathcal{H} = \sum_i V(B_i) + \sum_{i < j} A_{ij} B_i B_j \quad (M.10)$$

where  $V$  represents self-regulation and temperature measures the strength of demographic fluctuations. Studying the corresponding free energy landscape, in particular the complex structure of its global and local minima using the “replica trick,” allows predictions of phase transitions in this system (94, 95). We describe in supplementary materials, section S3.2 (54), how the boundary line between stable and unstable dynamics can be computed as a function of  $(\mu, \sigma)$  in the GLV and sublinear models. We show in fig. S7 the results of replica calculations for the sublinear model, which includes an additional density dependence term

such that  $p(B) = r(B/B_0)^{k-1} - rB/K$ , where  $K = 1$ . These results provide an alternative analytical approach to random matrix theory, but show a similarly increasing stability boundary with diversity [see the supplementary materials, section S4 (54)].

**Density threshold in the sublinear model**

The sublinear model with parameter  $B_0$  allows the growth rate,  $r$  to have dimension of 1/time. This permits  $r$  to be biologically meaningful and parameterized from auxiliary data that are available for maximum population growth rates (Fig. 5A). However, the sublinear model assumes that a near maximal growth rate is only possible at the minimum realistic population density, where any effects of crowding are negligible. Realistically, biomass cannot go to arbitrarily low values, below which, for example, the rate of encounter with a viable mate falls below mortality rate. At the extreme, when biomass approaches zero, sublinear growth approaches infinity, which is also unrealistic. Our theoretical results in Fig. 3 have considered  $B_0$  to be a simple normalization constant, with no change in behavior at  $B_i = B_0$ . However, if this constant is made to represent an extinction threshold, as was assumed for making macroecological predictions (see Fig. 5 and the subsection “Modeling abundance data,” below), then extinction can occur at high diversity or interaction strengths (fig. S5). Increasing these parameters ( $\mu$  and  $S$ ) suppresses the biomass of all species until the minimum species biomass  $B_i = B_0$  is reached, whereby it is removed from the community. Other low-density behaviors, such as a switch to exponential growth below a threshold (fig. S10), can also allow extinction at high  $\mu$  and  $S$ , but below this limit these behaviors do not qualitatively alter our findings of a positive diversity-stability relation.

**Production-biomass relations**

All empirical data in Fig. 4 have been previously published (64, 96–109) and most are summarized in (64) (figs. S14 and S15). In table S2 we report summary statistics for 39 production-biomass regressions, with raw data provided in supplementary data S1 [described in the supplementary materials, section S10 (54)]. For large mammal communities, herbivore community production is calculated from carnivore abundance and their per capita consumption, which closely aligns with estimates of herbivore community reproductive growth as outlined in (64). For the grassland and forest relations, we aggregate data from multiple large meta-analyses, each of which themselves reveal very similar production-biomass scaling. For invertebrates, we consider the populations of sometimes very different species resulting in wide residual variation, but similar scaling is also evident when populations

are aggregated into communities (64) and when disaggregated among the best represented genera (100) (listed in table S2). Fish include freshwater planktivore and benthivore populations, each of which is themselves significantly sublinear, but exclude higher trophic piscivores, which exhibit near linear growth (102, 104). For marine sediment bacteria, we chose to display only one of three groups examined in the original study (109), which was the most extensive and the only one to display a significant relation. This study (109) misreported the slope of their data, which is evident from their Fig. 1A, and we assume that the plotted data, rather than the regression statistics, are correct.

These data, spanning very different terrestrial and aquatic systems, include species that range from bacteria to large mammals and trees, representing some 20 orders of magnitude range in body mass. Therefore, the methods used to measure community biomass and production vary extensively and cannot be concisely summarized. Further information is available in (64) and in the references listed in table S4. Generally, the original studies all sought to estimate total community biomass and the maximum change in that biomass over representative spatial extents and temporal periods such that these data can be reasonably combined through simple unit conversions.

**Modeling production data**

We outline how the sublinear model is capable of recovering cross-ecosystem production versus biomass regressions (Fig. 4) [see the supplementary materials, section S7 (54)]. As mentioned, the GLV model with logistic growth can also recover these patterns but requires additional assumptions that appear unrealistic, so we defer details for the logistic growth model to the supplementary materials, section S9 (54).

The sublinear growth model is intended as a high-level description of a single interacting community within an ecosystem. However, it is relevant to consider what additional assumptions are needed to recover the cross-ecosystem patterns over different communities, as observed in Fig. 4. We consider the four focal groups of mammals, phytoplankton, invertebrates, and fish, for which extensive allometric and macroecological data exist. The full model for biomass density ( $g/m^2$ ) is written as

$$\frac{dB_i}{dt} = r_i B_i \left( \frac{B_i}{B_0} \right)^{k-1} \Theta(B_i - B_0) - z_i B_i - B_i \sum_{j \neq i} A_{ij} B_j \quad (M.11)$$

where  $B_0$  is the minimum biomass achievable by all species  $i$ . This extinction threshold sets the value at which per capita growth rate is at

a maximum  $r_i$  and below which growth is zero ( $\Theta$  denotes the Heaviside step function). All other parameters are as previously defined, except we now assume gamma-distributed  $A_{ij}$  to ensure purely competitive interactions (all  $A_{ij} > 0$ ). The dimensionality of terms can be summarized as follows:

$$\begin{aligned}
 [B_i] &= [B_0] = \frac{\text{mass}}{\text{area}}, \\
 [r_i] &= [z_i] = \frac{1}{\text{time}}, \\
 [A_{ij}] &= \frac{\text{area}}{\text{mass} \times \text{time}} \quad (\text{M.12})
 \end{aligned}$$

Other than the value of  $k$  (dimensionless), we estimate all parameter values for a given community type from independent data from those in Fig. 4. We make the following five assumptions, which we retain for modeling both the production-biomass relations (Fig. 4), and the four macroecological abundance patterns (see next subsection). First, we assume  $k = 3/4$  for all species. Second, we assume that diversity  $S$  is constant for each community type and arbitrarily set  $S = 50$ . Third, we assume that population parameters can be estimated from auxiliary data. Different species are characterized by different fixed intrinsic growth rates  $r_i$  and natural mortality rates  $z_i$  such that a given community type can be characterized by an average rate of growth  $r$  and mortality  $z$ . We estimate  $r$  and  $z$  as the geometric mean of all available individual reproductive growth and mortality rate data for each focal group independently from allometric data (15) (Fig. 5A). For mammals, phytoplankton, invertebrates, and fish, we obtain  $r$  values of 0.54, 490, 33, and 7.3, and  $z$  values of 0.17, 53, 3.0, and 0.25, respectively. Given the respective ratios of these values, we make a further simplifying assumption that  $z = r/10$ , which allows a single maximum biomass value for all species (see assumption 5, below). Fourth, we assume that the lower bound on biomass  $B_0$  is independent of body mass (15) and equivalent for all species  $i$ , which we estimate at  $0.01 \text{ g/m}^2$  (from Fig. 4) for all cross-community patterns. We model the within-community species abundance distribution (fig. S16) by fixing  $N_0$  constant across species [see the next subsection and (110–112)]. The upper bound on biomass  $B_{\text{max}}$  is obtained by assuming  $r \propto z$  (Fig. 5A), which gives a constant for all species,  $B_{\text{max}}$ , calculated as  $B_{\text{max}} = B_0(z/r)^{1/(k-1)}$  [see the supplementary materials, section S7 (54)]. Fifth, we model a biomass gradient, along which a community type exists, by varying interaction strengths  $\mu$  and  $\sigma$  in order that equilibrium biomass ranges between  $B_0$  and  $B_{\text{max}}$ . This can be achieved by varying  $\mu$  over the same  $r/B_0$ -scaled values for each community type. Lowering  $\mu$  increases  $B^*$  until natural mortality dominates over competition. We as-

sume  $\sigma/\mu = 1$ , which only affects the intercept of mean-variance scaling [see the next subsection and the supplementary materials, section S8 (54)]. Given the similar scaling of basal metabolism with maximum individual production (15, 67, 83), varying  $\mu$  on the same scale as growth rate ensures that interaction strengths may be metabolically relevant for the mean body size of each major taxonomic group (9, 28, 29, 40, 41).

**Modeling abundance data**

We tested the ability of the sublinear community model to recover other well-known macroecological abundance patterns. To do so, we use the same assumptions and parameter values that are used to model the production-biomass data (see previous subsection) to model abundance (Fig. 6). These patterns relate to the variation in abundance (Fig. 6, A and B) and how abundance relates to body mass (Fig. 6, C and D). We again focus on mammals, phytoplankton, invertebrates, and fish. Analytical derivations and results of simulations are shown in the supplementary materials, section S8 [logistic model abundance predictions are described in the supplementary materials, section S9 (54)]. All empirical data used to represent these patterns have been previously published and are summarized in table S3, with raw data provided in supplementary data S1 [see the supplementary materials, section S10 (54)] and references in table S4.

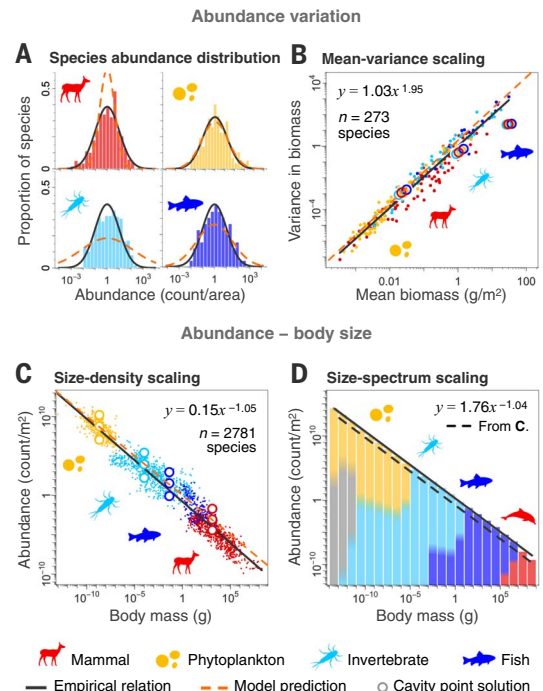
**Fig. 6. Modeling abundance patterns.**

Four macroecological patterns of abundance are shown across four taxonomic groups. Sublinear model solutions derive from the same set of parameters values and assumptions used previously (see Fig. 5 and the materials and methods). (A) The species abundance distribution is predicted to be log normal as obtained from the distribution of population growth rates within each major group (shown on RHS in Fig. 5B). The width is four times  $[1/(1 - k)]$  that of population growth rates and appears similar to the observed range of variation for each group. (B) Mean-variance scaling with an exponent of 2 is recovered when  $z = 0$ . Predictions deviate from power law scaling for finite  $z$  as  $B^*$  approaches  $B_{\text{max}}$  (colored circles). The intercept depends on  $\sigma/\mu$ , here assumed to be 1. (C) The size-density scaling prediction of  $-1$  (i.e.,  $N^* \sim m^{-1}$ ) is equivalent to biomass being independent of body mass (because  $r \sim z \sim m^{-3/4}$ , see Fig. 5A). The intercept is predicted to be 1 individual/ $\text{m}^2$ , and the empirical intercept is 0.15. The residual variation ranges from  $B_0$  to  $B_{\text{max}} = B_0(z/r)^{k-1}$  (i.e., four orders of magnitude; colored circles). (D) The size spectrum is shown averaged over the entire ocean to give size-class abundance in the same units as the population abundance of a species, shown in (C). The size spectrum is not explicitly modeled but requires that size-class diversity is invariant with body mass across locations in the ocean.

**Species abundance distribution**

The species abundance distribution is a within-community pattern of species commonness and rarity that is heavy-tailed and often best described by a lognormal distribution (66), although other distributions are also claimed, including the log-series, power law, and negative binomial, among others (13). Data in Fig. 6A derive from the following sources: mammals (globally) from (113), phytoplankton (Lake Biwa, Japan) from (114), and invertebrates (moths in Britain) and fish (Arabian Gulf) from (115). In Fig. 6A, each distribution is shown normalized with a geometric mean of one individual per unit area.

To model relative abundance within a given community, we assume a constant lower bound on abundance  $N_0$ , given this common observation from studies of particular communities (110–112, 115). We also assume the distribution of  $r_i$  values within a community type is comparable to the residual variation of the production-biomass regressions (shown on RHS in Fig. 5B; fig. S15 highlights the shape parameter). These assumptions give a log normal species abundance distribution  $P(N^*)$ , with a shape parameter (SD of the log of the variable) that is about four times  $[1/(1 - k) \approx 4]$  wider than that of the distribution of growth rates, depending on the value of  $k$  [see the supplementary materials, section S8.1, for analytical derivation (54)]. We thus obtain a long tail that is approximately within the



empirically observed range of variation reported for similar community types to our focal groups (Fig. 6A). Our model need not necessarily predict a log normal, but rather preserves the shape of the distribution of growth rates (when this is broad), extending the tail of the latter by  $1/(1 - k)$  and resulting in a relatively long-tailed distribution.

#### Mean-variance scaling

The variance in population abundance (or biomass, as shown in Fig. 6B) is known to scale as a power law with mean abundance, with exponents ranging from 1.5 to 2 for both temporal and spatial fluctuations of a species (also known as Taylor's law) (14, 116). Data in Fig. 6B include species biomass time series for 255 species from (15). We consider separate simulations as modeling a given community type across separate patches in space and compute the mean and variance in equilibrium biomass for each species.

We used the same assumptions listed in the previous subsection ("Modeling production data"). These assumptions give mean-variance scaling with exponent 2 when  $z \rightarrow 0$  [see the supplementary materials, section S8.2 (54)], but deviations from a power law are evident when  $z > 0$  as mean biomass approaches  $B_{\max}$  (open circles in Fig. 6B). The intercept is dependent on the value of  $\sigma/\mu$ , shown here set at 1 (Fig. 6B). We have also derived analytical results supporting these findings in the case where growth rates of a species are log normally distributed, [see the supplementary materials, section S8.2 (54)].

#### Size-density scaling

Size-density scaling is the relation of the average population density of a species versus average adult body mass across separate systems (also known as Damuth's law) (16). This relation is known to scale near  $-1$  across all species (15, 67), but with some 3 to 4 orders of magnitude residual variation in abundance. Data in Fig. 6C derive from (15). Again, we use the same above-listed assumptions (assumptions 1 to 5 in "Modeling production data"). Given that all growth and loss terms are assumed to scale in the same way (Fig. 5A) and the upper and lower bounds on biomass are independent of body mass, the corresponding bounds on numerical density should scale with body mass as  $m^{-1}$ . The model is thus consistent with the slope ( $= -1$ ), but also several other aspects of the size-density relation, including the intercept ( $= 1$  individual/ $m^2$ ) and the four-order residual variation [ $B_{\max}/B_0 = (z/r)^{1/(k-1)} = 10^4$ ] [see Fig. 6C and the supplementary materials, section S8.3 (54)].

#### Size-spectrum scaling

Size-spectrum scaling is the body size-frequency distribution within a community

(regardless of species identity) and is known to scale near  $-1$  within most aquatic systems for the relation of log abundance versus log size class (also known as the Sheldon spectrum) (68, 69). A similar scaling is evident for the complementary cumulative distribution function of body mass. Data in Fig. 6D are from (69), which estimated total ocean counts in each size class. We have transformed counts to density by dividing by ocean area ( $3.61 \times 10^{14} \text{ m}^2$ ) to show the correspondence between the size spectrum and the above-mentioned species size-density relation (Fig. 6C). Not only are the axes of each pattern equivalent, but slopes and intercepts are quite similar. The size spectrum, however, is a within-system univariate frequency distribution across size classes rather than a cross-system bivariate relation across species. Together, these patterns suggest that species diversity in a community should be independent of species body size, which may have some empirical support across metazoan taxa (117). Although we have not specifically modeled the size spectrum, our model is broadly consistent if we assume an invariance in size-class diversity.

#### Model simulations

Simulations of model behavior over a range of parameters served to validate our analytical results, as well as the robustness of our findings under different assumptions that were less amenable to formal analysis [see the supplementary materials, section S5 (54)]. Simulations were run by numerical integration of  $dB_i/dt = P_i(B_i) + C_i(B_1, \dots, B_S)$  using the Julia programming language, and all code is available at: <https://zenodo.org/doi/10.5281/zenodo.10476101>.

Parameter values for generating Fig. 2 are for a single species (top row of plots) and  $S = 15$  species (bottom row of plots), with the same population parameters,  $r = 1$  and  $z = 10^{-0.25}$ , and interaction matrix statistics,  $\mu = 0.1$  and  $\sigma = 0.01$ . Logistic growth assumes carrying capacity  $K = 10$ , whereas sublinear growth assumes  $k = 0.75$  for all species.

Parameter values used in Fig. 3 are the same across all plots (A to C), and we set the intrinsic growth rate  $r = 1$ , mortality  $z = 0$ , logistic carrying capacity  $K = 20$ , and sublinear scaling  $k = 3/4$ . Plot A is shown for  $\mu = 0.01$  and  $\sigma = 0.005$ . Plot B is shown for  $\mu = 0.005$  and  $\sigma = 0.0005$  and with  $S = 25, 50$ , and 100 species. Plot C shows these models generalized across parameters  $\mu$  and  $\sigma$  of the interaction matrix and diversity  $S$ , with the dashed black lines showing the  $\mu$  and  $\sigma$  values used in A and B. Logistic growth stability resides below the horizontal line at  $r/K = 0.05$ , whereas sublinear stability is below a positively increasing threshold (orange), which depends in part on  $k$ . Further information is available in the supplementary materials (54).

#### REFERENCES AND NOTES

- M. Loreau et al., Biodiversity and ecosystem functioning: Current knowledge and future challenges. *Science* **294**, 804–808 (2001). doi: [10.1126/science.1064088](https://doi.org/10.1126/science.1064088); PMID: [11679658](https://pubmed.ncbi.nlm.nih.gov/11679658/)
- K. V. Rosenberg et al., Decline of the North American avifauna. *Science* **366**, 120–124 (2019). doi: [10.1126/science.aaw1313](https://doi.org/10.1126/science.aaw1313); PMID: [31604313](https://pubmed.ncbi.nlm.nih.gov/31604313/)
- D. Storch et al., Biodiversity dynamics in the Anthropocene: How human activities change equilibria of species richness. *Ecography* **2022**, ecog.05778 (2022). doi: [10.1111/ecog.05778](https://doi.org/10.1111/ecog.05778)
- M. Loreau, A. Hector, F. Isbell, *The Ecological and Societal Consequences of Biodiversity Loss* (Wiley, 2022).
- R. M. May, Will a large complex system be stable? *Nature* **238**, 413–414 (1972). doi: [10.1038/238413a0](https://doi.org/10.1038/238413a0); PMID: [4559589](https://pubmed.ncbi.nlm.nih.gov/4559589/)
- R. M. May, Stability and complexity in model ecosystems. *Monogr. Popul. Biol.* **6**, 1–235 (1973). PMID: [4723571](https://pubmed.ncbi.nlm.nih.gov/4723571/)
- K. S. McCann, The diversity-stability debate. *Nature* **405**, 228–233 (2000). doi: [10.1038/35012234](https://doi.org/10.1038/35012234); PMID: [10821283](https://pubmed.ncbi.nlm.nih.gov/10821283/)
- P. Chesson, Mechanisms of maintenance of species diversity. *Annu. Rev. Ecol. Syst.* **31**, 343–366 (2000). doi: [10.1146/annurev.ecolsys.31.1.343](https://doi.org/10.1146/annurev.ecolsys.31.1.343)
- S. Allesina, S. Tang, Stability criteria for complex ecosystems. *Nature* **483**, 205–208 (2012). doi: [10.1038/nature10832](https://doi.org/10.1038/nature10832); PMID: [22343894](https://pubmed.ncbi.nlm.nih.gov/22343894/)
- G. Barabás, M. J. Michalska-Smith, S. Allesina, Self-regulation and the stability of large ecological networks. *Nat. Ecol. Evol.* **1**, 1870–1875 (2017). doi: [10.1038/s41598-017-0357-6](https://doi.org/10.1038/s41598-017-0357-6); PMID: [29062124](https://pubmed.ncbi.nlm.nih.gov/29062124/)
- J. Grilli, G. Barabás, M. J. Michalska-Smith, S. Allesina, Higher-order interactions stabilize dynamics in competitive network models. *Nature* **548**, 210–213 (2017). doi: [10.1038/nature23273](https://doi.org/10.1038/nature23273); PMID: [28746307](https://pubmed.ncbi.nlm.nih.gov/28746307/)
- L. Stone, The feasibility and stability of large complex biological networks: A random matrix approach. *Sci. Rep.* **8**, 8246 (2018). doi: [10.1038/s41598-018-26486-2](https://doi.org/10.1038/s41598-018-26486-2); PMID: [29844420](https://pubmed.ncbi.nlm.nih.gov/29844420/)
- B. J. McGill et al., Species abundance distributions: Moving beyond single prediction theories to integration within an ecological framework. *Ecol. Lett.* **10**, 995–1015 (2007). doi: [10.1111/j.1461-0248.2007.01094.x](https://doi.org/10.1111/j.1461-0248.2007.01094.x); PMID: [17845298](https://pubmed.ncbi.nlm.nih.gov/17845298/)
- L. R. Taylor, Aggregation, variance and the mean. *Nature* **189**, 732–735 (1961). doi: [10.1038/189732a0](https://doi.org/10.1038/189732a0)
- I. A. Hattton, A. P. Dobson, D. Storch, E. D. Galbraith, M. Loreau, Linking scaling laws across eukaryotes. *Proc. Natl. Acad. Sci. U.S.A.* **116**, 21616–21622 (2019). doi: [10.1073/pnas.1900492116](https://doi.org/10.1073/pnas.1900492116); PMID: [31591216](https://pubmed.ncbi.nlm.nih.gov/31591216/)
- J. Damuth, Population density and body size in mammals. *Nature* **290**, 699–700 (1981). doi: [10.1038/290699a0](https://doi.org/10.1038/290699a0)
- C. S. Elton, *The Ecology of Invasions by Animals and Plants* (Methue, 1958). doi: [10.1007/978-1-4899-7214-9](https://doi.org/10.1007/978-1-4899-7214-9)
- R. MacArthur, Fluctuations of animal populations and a measure of community stability. *Ecology* **36**, 533–536 (1955). doi: [10.2307/1929601](https://doi.org/10.2307/1929601)
- E. P. Odum, *Fundamentals of Ecology* (Saunders, 1959).
- R. Margalef, *Perspectives in Ecological Theory* (Univ. of Chicago Press, 1968).
- G. F. Gause, *The Struggle for Existence, 1934* (Williams & Wilkins, 1964).
- J. Hu, D. R. Amor, M. Barbier, G. Bunin, J. Gore, Emergent phases of ecological diversity and dynamics mapped in microcosms. *Science* **378**, 85–89 (2022). doi: [10.1126/science.abm7841](https://doi.org/10.1126/science.abm7841); PMID: [36201585](https://pubmed.ncbi.nlm.nih.gov/36201585/)
- A. Mougi, M. Kondoh, Diversity of interaction types and ecological community stability. *Science* **337**, 349–351 (2012). doi: [10.1126/science.1220529](https://doi.org/10.1126/science.1220529); PMID: [22822151](https://pubmed.ncbi.nlm.nih.gov/22822151/)
- G. Bunin, Ecological communities with Lotka-Volterra dynamics. *Phys. Rev. E* **95**, 042414 (2017). doi: [10.1103/PhysRevE.95.042414](https://doi.org/10.1103/PhysRevE.95.042414); PMID: [28505745](https://pubmed.ncbi.nlm.nih.gov/28505745/)
- A. Altieri, F. Roy, C. Cammarota, G. Biroli, Properties of equilibria and glassy phases of the random Lotka-Volterra model with demographic noise. *Phys. Rev. Lett.* **126**, 258301 (2021). doi: [10.1103/PhysRevLett.126.258301](https://doi.org/10.1103/PhysRevLett.126.258301); PMID: [34241496](https://pubmed.ncbi.nlm.nih.gov/34241496/)
- E. Johnson, A. Hastings, Resolving conceptual issues in Modern Coexistence Theory. [arXiv:2201.07926](https://arxiv.org/abs/2201.07926) [q-bio.PE] (2022).
- M. K. A. Gavina et al., Multi-species coexistence in Lotka-Volterra competitive systems with crowding effects. *Sci. Rep.* **8**, 1198 (2018). doi: [10.1038/s41598-017-19044-9](https://doi.org/10.1038/s41598-017-19044-9); PMID: [29352250](https://pubmed.ncbi.nlm.nih.gov/29352250/)
- U. Brose, R. J. Williams, N. D. Martinez, Allometric scaling enhances stability in complex food webs. *Ecol. Lett.* **9**,

- 1228–1236 (2006). doi: [10.1111/j.1461-0248.2006.00978.x](https://doi.org/10.1111/j.1461-0248.2006.00978.x); pmid: [17040325](https://pubmed.ncbi.nlm.nih.gov/17040325/)
29. P. Yodzis, The stability of real ecosystems. *Nature* **289**, 674–676 (1981). doi: [10.1038/289674a0](https://doi.org/10.1038/289674a0)
  30. R. P. Rohr, S. Saavedra, J. Bascompte, Ecological networks. On the structural stability of mutualistic systems. *Science* **345**, 1253497 (2014). doi: [10.1126/science.1253497](https://doi.org/10.1126/science.1253497); pmid: [25061214](https://pubmed.ncbi.nlm.nih.gov/25061214/)
  31. P. Yodzis, The connectance of real ecosystems. *Nature* **284**, 544–545 (1980). doi: [10.1038/284544a0](https://doi.org/10.1038/284544a0)
  32. J. Grilli, T. Rogers, S. Allesina, Modularity and stability in ecological communities. *Nat. Commun.* **7**, 12031 (2016). doi: [10.1038/ncomms12031](https://doi.org/10.1038/ncomms12031); pmid: [27337386](https://pubmed.ncbi.nlm.nih.gov/27337386/)
  33. P. P. Staniczenko, J. C. Kopp, S. Allesina, The ghost of nestlessness in ecological networks. *Nat. Commun.* **4**, 1391 (2013). doi: [10.1038/ncomms2422](https://doi.org/10.1038/ncomms2422); pmid: [23340431](https://pubmed.ncbi.nlm.nih.gov/23340431/)
  34. S. Allesina *et al.*, Predicting the stability of large structured food webs. *Nat. Commun.* **6**, 7842 (2015). doi: [10.1038/ncomms8842](https://doi.org/10.1038/ncomms8842); pmid: [26198207](https://pubmed.ncbi.nlm.nih.gov/26198207/)
  35. C. A. Serván, J. A. Capitán, J. Grilli, K. E. Morrison, S. Allesina, Coexistence of many species in random ecosystems. *Nat. Ecol. Evol.* **2**, 1237–1242 (2018). doi: [10.1038/s41559-018-0603-6](https://doi.org/10.1038/s41559-018-0603-6); pmid: [29988167](https://pubmed.ncbi.nlm.nih.gov/29988167/)
  36. G. Barabás, M. J. Michalaska-Smith, S. Allesina, The effect of intra- and interspecific competition on coexistence in multispecies communities. *Am. Nat.* **188**, E1–E12 (2016). doi: [10.1086/686901](https://doi.org/10.1086/686901); pmid: [27322128](https://pubmed.ncbi.nlm.nih.gov/27322128/)
  37. K. McCann, A. Hastings, G. R. Huxel, Weak trophic interactions and the balance of nature. *Nature* **395**, 794–798 (1998). doi: [10.1038/27427](https://doi.org/10.1038/27427)
  38. D. Tilman, *Resource Competition and Community Structure* (Princeton Univ. Press, 1982).
  39. P. B. Adler *et al.*, Competition and coexistence in plant communities: Intraspecific competition is stronger than interspecific competition. *Ecol. Lett.* **21**, 1319–1329 (2018). doi: [10.1111/ele.13098](https://doi.org/10.1111/ele.13098); pmid: [29938882](https://pubmed.ncbi.nlm.nih.gov/29938882/)
  40. P. Yodzis, S. Innes, Body size and consumer-resource dynamics. *Am. Nat.* **139**, 1151–1175 (1992). doi: [10.1086/285380](https://doi.org/10.1086/285380)
  41. S. Tang, S. Pawar, S. Allesina, Correlation between interaction strengths drives stability in large ecological networks. *Ecol. Lett.* **17**, 1094–1100 (2014). doi: [10.1111/ele.12312](https://doi.org/10.1111/ele.12312); pmid: [24946877](https://pubmed.ncbi.nlm.nih.gov/24946877/)
  42. E. Bairéy, E. D. Kelsic, R. Kishony, High-order species interactions shape ecosystem diversity. *Nat. Commun.* **7**, 12285 (2016). doi: [10.1038/ncomms12285](https://doi.org/10.1038/ncomms12285); pmid: [27481625](https://pubmed.ncbi.nlm.nih.gov/27481625/)
  43. S. Zaoli, A. Giometto, A. Maritan, A. Rinaldo, Covariations in ecological scaling laws fostered by community dynamics. *Proc. Natl. Acad. Sci. U.S.A.* **114**, 10672–10677 (2017). doi: [10.1073/pnas.1708376114](https://doi.org/10.1073/pnas.1708376114); pmid: [28830995](https://pubmed.ncbi.nlm.nih.gov/28830995/)
  44. S. P. Hubbell, “The unified neutral theory of biodiversity and biogeography (MPB-32)” in *The Unified Neutral Theory of Biodiversity and Biogeography* (MPB-32) (Princeton Univ. Press, 2011), vol. 32 in *Monographs in Population Biology*, pp. XX–XX. doi: [10.1515/9781400837526](https://doi.org/10.1515/9781400837526)
  45. L. N. Hudson, D. C. Reuman, A cure for the plague of parameters: Constraining models of complex population dynamics with allometries. *Proc. Biol. Sci.* **280**, 20131901 (2013). doi: [10.1098/rspb.2013.1901](https://doi.org/10.1098/rspb.2013.1901); pmid: [24026824](https://pubmed.ncbi.nlm.nih.gov/24026824/)
  46. S. Pawar, A. I. Dell, V. M. Savage, Dimensionality of consumer search space drives trophic interaction strengths. *Nature* **486**, 485–489 (2012). doi: [10.1038/nature11131](https://doi.org/10.1038/nature11131); pmid: [22722834](https://pubmed.ncbi.nlm.nih.gov/22722834/)
  47. J. P. DeLong, D. A. Vasseur, A dynamic explanation of size-density scaling in carnivores. *Ecology* **93**, 470–476 (2012). doi: [10.1890/11-1138.1](https://doi.org/10.1890/11-1138.1); pmid: [22624202](https://pubmed.ncbi.nlm.nih.gov/22624202/)
  48. L. von Bertalanffy, Quantitative laws in metabolism and growth. *Q. Rev. Biol.* **32**, 217–231 (1957). doi: [10.1086/401873](https://doi.org/10.1086/401873); pmid: [13485376](https://pubmed.ncbi.nlm.nih.gov/13485376/)
  49. R. E. Ricklefs, Is rate of ontogenetic growth constrained by resource supply or tissue growth potential? A comment on West *et al.*'s model. *Funct. Ecol.* **17**, 384–393 (2003). doi: [10.1046/j.1365-2435.2003.00745.x](https://doi.org/10.1046/j.1365-2435.2003.00745.x)
  50. C. Hou *et al.*, Energy uptake and allocation during ontogeny. *Science* **322**, 736–739 (2008). doi: [10.1126/science.1162302](https://doi.org/10.1126/science.1162302); pmid: [18974352](https://pubmed.ncbi.nlm.nih.gov/18974352/)
  51. G. B. West, J. H. Brown, B. J. Enquist, A general model for ontogenetic growth. *Nature* **413**, 628–631 (2001). doi: [10.1038/35098076](https://doi.org/10.1038/35098076); pmid: [11675785](https://pubmed.ncbi.nlm.nih.gov/11675785/)
  52. E. M. Zullinger, R. E. Ricklefs, K. H. Redford, G. M. Mace, Fitting Sigmoidal Equations to Mammalian Growth Curves. *J. Mammal.* **65**, 607–636 (1984). doi: [10.2307/1380844](https://doi.org/10.2307/1380844)
  53. I. Hatton, “What regulates growth across levels of organization?” in *Unsolved Problems in Ecology*, A. Dobson, R. Holt, D. Tilman, Eds. (Princeton Univ. Press, 2020), pp. 203–217. doi: [10.2307/j.ctvcs9fh2n.20](https://doi.org/10.2307/j.ctvcs9fh2n.20)
  54. Further details are provided in the materials and methods section of the supplementary materials.
  55. M. E. Gilpin, F. J. Ayala, Global models of growth and competition. *Proc. Natl. Acad. Sci. U.S.A.* **70**, 3590–3593 (1973). doi: [10.1073/pnas.70.12.3590](https://doi.org/10.1073/pnas.70.12.3590); pmid: [4519647](https://pubmed.ncbi.nlm.nih.gov/4519647/)
  56. F. J. Richards, A flexible growth function for empirical use. *J. Exp. Bot.* **10**, 290–301 (1959). doi: [10.1093/jxb/10.2.290](https://doi.org/10.1093/jxb/10.2.290)
  57. R. M. Sibly, D. Barker, M. C. Denham, J. Hone, M. Pagel, On the regulation of populations of mammals, birds, fish, and insects. *Science* **309**, 607–610 (2005). doi: [10.1126/science.1110760](https://doi.org/10.1126/science.1110760); pmid: [16040705](https://pubmed.ncbi.nlm.nih.gov/16040705/)
  58. F. E. Smith, Population dynamics in *Daphnia magna* and a new model for population growth. *Ecology* **44**, 651–663 (1963). doi: [10.2307/1933011](https://doi.org/10.2307/1933011)
  59. R. M. Sibly, J. Hone, Population growth rate and its determinants: An overview. *Philos. Trans. R. Soc. Lond. B Biol. Sci.* **357**, 1153–1170 (2002). doi: [10.1098/rstb.2002.1117](https://doi.org/10.1098/rstb.2002.1117); pmid: [12396508](https://pubmed.ncbi.nlm.nih.gov/12396508/)
  60. B.-E. Saether, S. Engen, E. Matthysen, Demographic characteristics and population dynamical patterns of solitary birds. *Science* **295**, 2070–2073 (2002). doi: [10.1126/science.1068766](https://doi.org/10.1126/science.1068766); pmid: [11896278](https://pubmed.ncbi.nlm.nih.gov/11896278/)
  61. A. Borlestean, P. C. Frost, D. L. Murray, A mechanistic analysis of density dependence in algal population dynamics. *Front. Ecol. Evol.* **3**, 00037 (2015). doi: [10.3389/fevo.2015.00037](https://doi.org/10.3389/fevo.2015.00037)
  62. L. A. Sauer, K. E. Hawes, S. A. Juliano, Non-linear relationships between density and demographic traits in three *Aedes* species. *Sci. Rep.* **12**, 8075 (2022). doi: [10.1038/s41598-022-11909-y](https://doi.org/10.1038/s41598-022-11909-y); pmid: [35577868](https://pubmed.ncbi.nlm.nih.gov/35577868/)
  63. M. Barbier, C. de Mazancourt, M. Loreau, G. Bunin, Fingerprints of high-dimensional coexistence in complex ecosystems. *Phys. Rev. X* **11**, 011009 (2021). doi: [10.1103/PhysRevX.11.011009](https://doi.org/10.1103/PhysRevX.11.011009)
  64. I. A. Hatton *et al.*, The predator-prey power law: Biomass scaling across terrestrial and aquatic biomes. *Science* **349**, aac6284 (2015). doi: [10.1126/science.aac6284](https://doi.org/10.1126/science.aac6284); pmid: [26339034](https://pubmed.ncbi.nlm.nih.gov/26339034/)
  65. D. M. Perkins *et al.*, Consistent predator-prey biomass scaling in complex food webs. *Nat. Commun.* **13**, 4990 (2022). doi: [10.1038/s41467-022-32578-5](https://doi.org/10.1038/s41467-022-32578-5); pmid: [36008387](https://pubmed.ncbi.nlm.nih.gov/36008387/)
  66. F. W. Preston, The commonness, and rarity, of species. *Ecology* **29**, 254–283 (1948). doi: [10.2307/1930989](https://doi.org/10.2307/1930989)
  67. R. H. Peters, *The Ecological Implications of Body Size* (Cambridge Univ. Press, 1983).
  68. R. W. Sheldon, A. Prakash, W. H. Sutcliffe Jr., The size distribution of particles in the ocean. *Limnol. Oceanogr.* **17**, 327–340 (1972). doi: [10.4319/lo.1972.17.3.0327](https://doi.org/10.4319/lo.1972.17.3.0327)
  69. I. A. Hatton, R. F. Heneghan, Y. M. Bar-On, E. D. Galbraith, The global ocean size spectrum from bacteria to whales. *Sci. Adv.* **7**, eabh3732 (2021). doi: [10.1126/sciadv.abh3732](https://doi.org/10.1126/sciadv.abh3732); pmid: [34757796](https://pubmed.ncbi.nlm.nih.gov/34757796/)
  70. J. Grilli, Macroecological laws describe variation and diversity in microbial communities. *Nat. Commun.* **11**, 4743 (2020). doi: [10.1038/s41467-020-18529-y](https://doi.org/10.1038/s41467-020-18529-y); pmid: [32958773](https://pubmed.ncbi.nlm.nih.gov/32958773/)
  71. C. S. Holling, Resilience and stability of ecological systems. *Annu. Rev. Ecol. Syst.* **4**, 1–23 (1973). doi: [10.1146/annurev.es.04.110173.000245](https://doi.org/10.1146/annurev.es.04.110173.000245)
  72. F. van der Plas, Biodiversity and ecosystem functioning in naturally assembled communities. *Biol. Rev. Camb. Philos. Soc.* **94**, 1220–1245 (2019). doi: [10.1111/brv.12499](https://doi.org/10.1111/brv.12499); pmid: [30724447](https://pubmed.ncbi.nlm.nih.gov/30724447/)
  73. B. Worm *et al.*, Impacts of biodiversity loss on ocean ecosystem services. *Science* **314**, 787–790 (2006). doi: [10.1126/science.1132294](https://doi.org/10.1126/science.1132294); pmid: [17082450](https://pubmed.ncbi.nlm.nih.gov/17082450/)
  74. T. B. Reusch, A. Ehlers, A. Hämmel, B. Worm, Ecosystem recovery after climatic extremes enhanced by genotypic diversity. *Proc. Natl. Acad. Sci. U.S.A.* **102**, 2826–2831 (2005). doi: [10.1073/pnas.050008102](https://doi.org/10.1073/pnas.050008102); pmid: [15710890](https://pubmed.ncbi.nlm.nih.gov/15710890/)
  75. D. Tilman, J. A. Downing, Biodiversity and stability in grasslands. *Nature* **367**, 363–365 (1994). doi: [10.1038/367363a0](https://doi.org/10.1038/367363a0)
  76. J. M. Fryxell *et al.*, Stabilizing effects of group formation by Serengeti herbivores on predator-prey dynamics. *Front. Ecol. Evol.* **10**, 981842 (2022). doi: [10.3389/fevo.2022.981842](https://doi.org/10.3389/fevo.2022.981842)
  77. R. W. Wrangham, J. L. Gittleman, C. A. Chapman, Constraints on group size in primates and carnivores: Population density and day-range as assays of exploitation competition. *Behav. Ecol. Sociobiol.* **32**, 199–209 (1993). doi: [10.1007/BF00173778](https://doi.org/10.1007/BF00173778)
  78. L. Keller, H. K. Reeve, Partitioning of reproduction in animal societies. *Trends Ecol. Evol.* **9**, 98–102 (1994). doi: [10.1016/0169-5347\(94\)90204-6](https://doi.org/10.1016/0169-5347(94)90204-6); pmid: [21236786](https://pubmed.ncbi.nlm.nih.gov/21236786/)
  79. M. Westoby, Self-thinning driven by leaf area not by weight. *Nature* **265**, 330–331 (1977). doi: [10.1038/265330a0](https://doi.org/10.1038/265330a0)
  80. T. Gibbs, Y. Zhang, Z. R. Miller, J. P. O'Dwyer, Stability criteria for the consumption and exchange of essential resources. *PLOS Comput. Biol.* **18**, e1010521 (2022). doi: [10.1371/journal.pcbi.1010521](https://doi.org/10.1371/journal.pcbi.1010521); pmid: [36074781](https://pubmed.ncbi.nlm.nih.gov/36074781/)
  81. T. J. Case, On the evolution and adaptive significance of postnatal growth rates in the terrestrial vertebrates. *Q. Rev. Biol.* **53**, 243–282 (1978). doi: [10.1086/410622](https://doi.org/10.1086/410622); pmid: [362471](https://pubmed.ncbi.nlm.nih.gov/362471/)
  82. T. Fenchel, Intrinsic rate of natural increase: The relationship with body size. *Oecologia* **14**, 317–326 (1974). doi: [10.1007/BF00384576](https://doi.org/10.1007/BF00384576); pmid: [28308657](https://pubmed.ncbi.nlm.nih.gov/28308657/)
  83. J. H. Brown, J. F. Gillooly, A. P. Allen, V. M. Savage, G. B. West, Toward a metabolic theory of ecology. *Ecology* **85**, 1771–1789 (2004). doi: [10.1890/03-9000](https://doi.org/10.1890/03-9000)
  84. D. S. Glazier, Is metabolic rate a universal ‘pacemaker’ for biological processes? *Biol. Rev. Camb. Philos. Soc.* **90**, 377–407 (2015). doi: [10.1111/brv.12115](https://doi.org/10.1111/brv.12115); pmid: [24863680](https://pubmed.ncbi.nlm.nih.gov/24863680/)
  85. C. Hou, M. Kaspari, H. B. Vander Zanden, J. F. Gillooly, Energetic basis of colonial living in social insects. *Proc. Natl. Acad. Sci. U.S.A.* **107**, 3634–3638 (2010). doi: [10.1073/pnas.0908071107](https://doi.org/10.1073/pnas.0908071107); pmid: [20133582](https://pubmed.ncbi.nlm.nih.gov/20133582/)
  86. B. Gompertz, On the nature of the function expressive of the law of human mortality, and on a new mode of determining the value of life contingencies. In a letter to Francis Baily, Esq. F. R. S. & C. *Philos. Trans. R. Soc. Lond.* **115**, 513–583 (1825). doi: [10.1098/rstl.1825.0026](https://doi.org/10.1098/rstl.1825.0026)
  87. K. M. C. Tjørve, E. Tjørve, The use of Gompertz models in growth analyses, and new Gompertz-model approach: An addition to the Unified-Richards family. *PLOS ONE* **12**, e0178691 (2017). doi: [10.1371/journal.pone.0178691](https://doi.org/10.1371/journal.pone.0178691); pmid: [28582419](https://pubmed.ncbi.nlm.nih.gov/28582419/)
  88. T. Tahara *et al.*, Asymptotic stability of a modified Lotka-Volterra model with small immigrations. *Sci. Rep.* **8**, 7029 (2018). doi: [10.1038/s41598-018-25436-2](https://doi.org/10.1038/s41598-018-25436-2); pmid: [29728625](https://pubmed.ncbi.nlm.nih.gov/29728625/)
  89. S. R. Serrao, U. C. Täuber, Stabilizing spiral structures and population diversity in the asymmetric May–Leonard model through immigration. *Eur. Phys. J. B* **94**, 175 (2021). doi: [10.1140/epjb/s10051-021-00168-x](https://doi.org/10.1140/epjb/s10051-021-00168-x)
  90. F. Clark, B. W. Brook, S. Delean, H. Reşit Akçakaya, C. J. A. Bradshaw, The theta-logistic is unreliable for modelling most census data. *Methods Ecol. Evol.* **1**, 253–262 (2010). doi: [10.1111/j.2041-210X.2010.00029.x](https://doi.org/10.1111/j.2041-210X.2010.00029.x)
  91. National Environment Research Council (NERC) Centre for Population Biology, *Imperial College, Global Population Dynamics Database* (NERC, 1999).
  92. J. Prendergast, E. Bazeley-White, O. Smith, J. Lawton, P. Inchausti, D. Kidd, S. Knight, “The Global Population Dynamics Database” (2010); <https://knbc.ecoinformatics.org/view/doi:10.5063/F1B263Z8>.
  93. Y. Ahmadian, F. Fumarola, K. D. Miller, Properties of networks with partially structured and partially random connectivity. *Phys. Rev. E Stat. Nonlin. Soft Matter Phys.* **91**, 012820 (2015). doi: [10.1103/PhysRevE.91.012820](https://doi.org/10.1103/PhysRevE.91.012820); pmid: [25679669](https://pubmed.ncbi.nlm.nih.gov/25679669/)
  94. G. Biroli, G. Bunin, C. Cammarota, Marginally stable equilibria in critical ecosystems. *New J. Phys.* **20**, 083051 (2018). doi: [10.1088/1367-2630/aad588](https://doi.org/10.1088/1367-2630/aad588)
  95. A. Altieri, G. Biroli, Effects of intraspecific cooperative interactions in large ecosystems. *SciPost Phys.* **12**, 013 (2022). doi: [10.21468/SciPostPhys.12.1.013](https://doi.org/10.21468/SciPostPhys.12.1.013)
  96. H. Cyr, R. H. Peters, Biomass-size spectra and the prediction of fish biomass in lakes. *Can. J. Fish. Aquat. Sci.* **53**, 994–1006 (1996). doi: [10.1139/f96-033](https://doi.org/10.1139/f96-033)
  97. M. A. Huston, S. Wolverton, The global distribution of net primary production: Resolving the paradox. *Ecol. Monogr.* **79**, 343–377 (2009). doi: [10.1890/08-0588.1](https://doi.org/10.1890/08-0588.1)
  98. S. T. Michaletz, D. Cheng, A. J. Kerkhoff, B. J. Enquist, Convergence of terrestrial plant production across global climate gradients. *Nature* **512**, 39–43 (2014). doi: [10.1038/nature13470](https://doi.org/10.1038/nature13470); pmid: [25043056](https://pubmed.ncbi.nlm.nih.gov/25043056/)

99. K. J. Niklas, B. J. Enquist, "Biomass allocation and growth data of seeded plants" (ORNL DAAC, 2004); [https://daac.ornl.gov/cgi-bin/dsviewer.pl?ds\\_id=703](https://daac.ornl.gov/cgi-bin/dsviewer.pl?ds_id=703).
100. C. Plante, J. A. Downing, Production of freshwater invertebrate populations in lakes. *Can. J. Fish. Aquat. Sci.* **46**, 1489–1498 (1989). doi: [10.1139/f189-191](https://doi.org/10.1139/f189-191)
101. K. Banse, S. Mosher, Adult body mass and annual production/ biomass relationships of field populations. *Ecol. Monogr.* **50**, 355–379 (1980). doi: [10.2307/2937256](https://doi.org/10.2307/2937256)
102. J. A. Downing, C. Plante, Production of fish populations in lakes. *Can. J. Fish. Aquat. Sci.* **50**, 110–120 (1993). doi: [10.1139/f93-013](https://doi.org/10.1139/f93-013)
103. J. A. Downing, C. Plante, S. Lalonde, Fish production correlated with primary productivity, not the morphoedaphic index. *Can. J. Fish. Aquat. Sci.* **47**, 1929–1936 (1990). doi: [10.1139/f90-217](https://doi.org/10.1139/f90-217)
104. R. G. Randall, C. K. Minns, J. R. M. Kelso, Fish production in freshwaters: Are rivers more productive than lakes? *Can. J. Fish. Aquat. Sci.* **52**, 631–643 (1995). doi: [10.1139/f95-063](https://doi.org/10.1139/f95-063)
105. C. M. Duarte, C. L. Chiscano, Seagrass biomass and production: A reassessment. *Aquat. Bot.* **65**, 159–174 (1999). doi: [10.1016/S0304-3770\(99\)00038-8](https://doi.org/10.1016/S0304-3770(99)00038-8)
106. R. T. Coupland, *Natural Grasslands: Eastern Hemisphere and Résumé* (Elsevier Science, 1993), vol. 8B.
107. P. L. Sims, J. S. Singh, W. K. Lauenroth, The structure and function of ten western North American grasslands: I. Abiotic and vegetational characteristics. *J. Ecol.* **66**, 251–285 (1978). doi: [10.2307/2259192](https://doi.org/10.2307/2259192)
108. M. Rychnovska, "Ecosystem synthesis of meadows" in *Grassland Ecosystems of the World: Analysis of Grasslands and Their Uses*, R. T. Coupland, Ed. (Cambridge University Press, 1979), pp. 165–169.
109. B. C. Sander, J. Kalff, Factors controlling bacterial production in marine and freshwater sediments. *Microb. Ecol.* **26**, 79–99 (1993). doi: [10.1007/BF00177045](https://doi.org/10.1007/BF00177045); pmid: [24190006](https://pubmed.ncbi.nlm.nih.gov/24190006/)
110. P. Cotgreave, The relationship between body size and population abundance in animals. *Trends Ecol. Evol.* **8**, 244–248 (1993). doi: [10.1016/0169-5347\(93\)90199-Y](https://doi.org/10.1016/0169-5347(93)90199-Y); pmid: [21236159](https://pubmed.ncbi.nlm.nih.gov/21236159/)
111. E. P. White, S. K. Ernest, A. J. Kerkhoff, B. J. Enquist, Relationships between body size and abundance in ecology. *Trends Ecol. Evol.* **22**, 323–330 (2007). doi: [10.1016/j.tree.2007.03.007](https://doi.org/10.1016/j.tree.2007.03.007); pmid: [17399851](https://pubmed.ncbi.nlm.nih.gov/17399851/)
112. T. M. Blackburn *et al.*, The relationship between abundance and body size in natural animal assemblages. *J. Anim. Ecol.* **62**, 519–528 (1993). doi: [10.2307/5201](https://doi.org/10.2307/5201)
113. K. E. Jones *et al.*, PanTHERIA: A species-level database of life history, ecology, and geography of extant and recently extinct mammals. *Ecology* **90**, 2648–2648 (2009). doi: [10.1890/08-1494.1](https://doi.org/10.1890/08-1494.1)
114. C.-H. Tsai *et al.*, Phytoplankton functional group dynamics explain species abundance distribution in a directionally changing environment. *Ecology* **95**, 3335–3343 (2014). doi: [10.1890/13-1946.1](https://doi.org/10.1890/13-1946.1)
115. A. E. Magurran, *Measuring Biological Diversity* (, 2003).
116. Z. Eisler, I. Bartos, J. Kertesz, Fluctuation scaling in complex systems: Taylor's law and beyond. *Adv. Phys.* **57**, 89–142 (2008). doi: [10.1080/00018730801893043](https://doi.org/10.1080/00018730801893043)
117. C. D. L. Orme, D. L. J. Quicke, J. M. Cook, A. Purvis, Body size does not predict species richness among the metazoan phyla. *J. Evol. Biol.* **15**, 235–247 (2002). doi: [10.1046/j.1420-9101.2002.00379.x](https://doi.org/10.1046/j.1420-9101.2002.00379.x)
118. I. A. Hatton, O. Mazzarisi, A. Altieri, M. Smerlak, Code for: Diversity begets stability: sublinear growth and competitive coexistence across ecosystems, Zenodo (2024); <https://zenodo.org/doi/10.5281/zenodo.10476101>.

#### ACKNOWLEDGMENTS

We are especially grateful to M. Barbier, D. C. Reuman, and E. D. Galbraith for discussion and feedback. We also thank

J.-P. Bouchaud, U. Brose, G. Bunin, J. Grilli, M. Loreau, K. S. McCann, D. Storch, A. Zadorin, J. Yoshimura, S. Pawar, and S. Allesina for valuable comments on an earlier draft of the manuscript and R. M. Sibly and D. Barker for sharing data. **Funding:** This work was supported by the Alexander von Humboldt Foundation in the framework of the Sofja Kovalevskaja Award endowed by the German Federal Ministry of Education and Research (M.S., O.M.), by an Alexander von Humboldt Research Fellowship (I.A.H.), and by the National Science Foundation (NSF BIO OCE grant 2023474 to O.M.). **Author contributions:** I.A.H. and M.S. conceived the study. All authors analyzed data, performed theoretical modeling, and wrote the manuscript. **Competing interests:** The authors declare no competing interests. **Data and materials availability:** All data are available in data S1 of supplementary materials and in (92, 113). References for data sources can be found in table S4 of the supplementary materials. All code used for simulation and analysis is available at Zenodo (118). **License information:** Copyright © 2024 the authors, some rights reserved; exclusive licensee American Association for the Advancement of Science. No claim to original US government works. <https://www.science.org/about/science-licenses-journal-article-reuse>

#### SUPPLEMENTARY MATERIALS

[science.org/doi/10.1126/science.adg8488](https://science.org/doi/10.1126/science.adg8488)

Materials and Methods

Supplementary Text

Figs. S1 to S18

Tables S1 to S4

References (119–223)

Data S1

Submitted 25 January 2023; resubmitted 9 August 2023

Accepted 7 February 2024

[10.1126/science.adg8488](https://doi.org/10.1126/science.adg8488)